MODELING AND CONTROL OF INTERCONNECTED HYDRAULIC WIND TURBINES

A Thesis

Submitted to the Faculty

of

Purdue University

by

Aryan Asgharifard

In Partial Fulfillment of the

Requirements for the Degree

of

Master of Science in Mechanical Engineering

August 2018

Purdue University

Indianapolis, Indiana

THE PURDUE UNIVERSITY GRADUATE SCHOOL
STATEMENT OF COMMITTEE APPROVAL

Dr. Afshin Izadian, Co-Chair

School of Engineering Technology - Indianapolis

Dr. Sohel Anwar, Co-Chair

Department of Mechanical and Energy Engineering

Dr. Hamid Dalir

Department of Mechanical and Energy Engineering

Approved by:

Dr. Jie Chen

Head of the Graduate Program

Bunu anneme, babama ve kardeşime adamak istiyorum. Onsuz olsaydı bu mümkün olmazdı.

ACKNOWLEDGMENTS

I would like to thank Dr. Afshin Izadian for this exceptional learning and research opportunity along with his endless intellectual and financial support during my master's degree, and provisions above the academic contexts. I would like to thank Dr. Sohel Anwar for all his academic and financial support during my studies. I would like to thank my committee members for their assistance and supervision in preparation of this thesis. Finally, I reserve special gratitude for my family, for their limitless mental and financial support.

PREFACE

The role of renewable energies are becoming increasingly significant in our daily lives since we are beginning to observe the consequences of the fossil fuels and greenhouse gases in our planet. Therefore, any work towards the development of improved technologies and equipments that can harvest more of renewable energies is a step making our planet independent of nonrenewable and polluting fuels. In the following chapters, I have discussed and provided the results in developing and improving the hydraulic wind power transfer system, a system that provides us with significantly cheaper alternative to conventional wind turbines.

TABLE OF CONTENTS

Page

LIST OF TABLES

LIST OF FIGURES

Figure Page

SYMBOLS

P	power
V	velocity
$\dot{m}$	mass flow rate
ρ	density
C_P	power coefficient
λ	tip-speed ratio
θ	pitch angle
A	swept area
R	blade radius
ω	angular velocity
T	temperature
τ	torque
Q	volumetric flow rate
D	displacement volume
p	pressure
η	efficiency
J	moment of inertia
k	ratio of heat capacities
β	compression/expansion ratio

ABBREVIATIONS

HWPTS	Hydraulic Wind Power Transfer System
CAES	Compressed Air Energy Storage
MPP	Maximum Power Point
MPPT	Maximum Power Point Tracking

ABSTRACT

Asgharifard, Aryan. M.S.M.E., Purdue University, August 2018. Modeling and Control of Interconnected Hydraulic Wind Turbines. Major Professors: Afshin Izadian and Sohel Anwar

Hydraulic Wind Power Transfer System is a promising alternative to conventional wind turbines, and an increased research in this field indicates the ability of this technology to replace conventional wind turbines. This technology not only provides an initial economical advantage by eliminating the need for a gearbox unit, but also provides further long term economical and reliability advantage by transferring the generation unit to the ground level, which provides a low-cost and easier maintenance and inspection. In addition, transferring the generation unit to the ground level and eliminating the gearbox decreases the weight of the wind turbine and thus reducing the size of the foundation.

However, the unpredictability of renewable energies make them less reliable and prone to power shortage. To mitigate this issue, an energy storage system can be coupled to the generation system so that it would store the excess energy when the renewable source has more power than the demand, and return the excess energy back to the system when the renewable source is not able to meet the demand.

Similar to conventional wind turbines, this technology also requires complex control algorithms to operate. These algorithms not only aim to improve the power quality and match the grid rules, but also aim to absorb the maximum amount of power from wind. To design proper control strategies, a detailed model of the system is needed for the simulation.

During my research in this lab, my contributions included: (1) Introduction of a method to eliminate the need for proportional valve for frequency control and thus

eliminating the valve pressure loss in the hydraulic wind power system (2) Integration of a energy storage system with the hydraulic system and design of a control system in order to maintain the generator frequency during power shortage (3) Proposal of an strategy and control method for Maximum Power Point Tracking (MPPT) and increasing the efficiency of the wind power absorption. Besides these mentioned points, I have also conducted simulations and have revised methods for wind speed estimation, and use of neural-networks to optimize the generators. However, due to time constraint or unfinished work, I have included them as recommendations for future research.

1. INTRODUCTION

1.1 Wind Energy

As stated by the U.N. Brundtland Commission, sustainable energy is the provision of energy such that it meets all the needs of the present without compromising the ability of future generations to meet their own needs [1]. Renewable energy is one of the pillars of sustainable energy, which includes sources such as solar energy, hydro-electricity energy, and wind energy. Technological advancements in renewable energy area has prompted us to build larger and more efficient structures and components to facilitate the independence from fossil fuel sources even further.

Wind power is the use of air flow through wind turbines to run the generators to produce electricity. Wind power is clean, emission-free, and occupies little land. By the end of 2016,over 90 countries had seen commercial wind activity, and 29 countries had more than 1 GW in operation. Wind has become the least-expensive option for new power generation in an increasing number of countries [2]. Currently, China has the largest wind power capacity of close to 200 Gigawatts, followed by United States with a capacity of about 82 Gigawatts, followed by Germany with about 50 Gigawatts wind power capacity. However, the top three countries that meet the highest share of their electricity demand by wind power are Denmark, with about 40%, Ireland, with about 30%, and Portugal, with close to 25% [2]. As shown in Fig 1.1, the global wind power capacity has increased almost exponentially in the past decade.

In United States, cumulative U.S. wind power grew by 11%, representing 27% of all new capacity additions in 2016 [2]. Wind energy has supported over 100,000 jobs across America related to project development, siting, turbine manufacturing, etc. in 2016, with about 32% increase from the previous year [3]. In addition, United States is currently providing over 6% of its annual electricity demand through wind power,

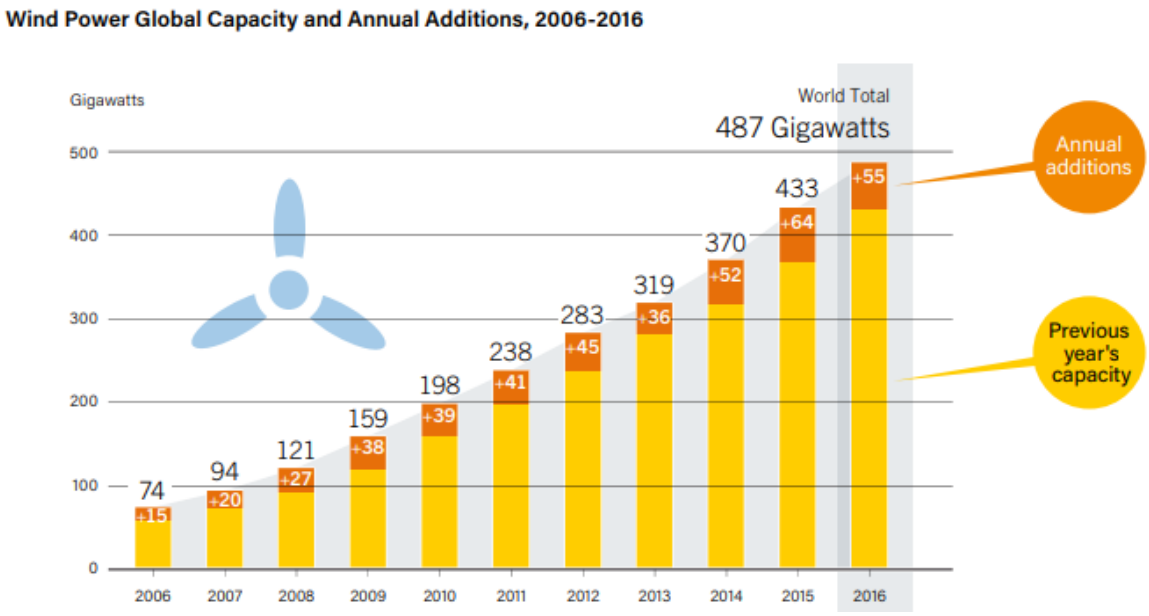

Fig. 1.1. Global capacity of wind power in the last decade [2]

with Texas leading the nation with over 20 Gigawatts power. In December 2016, the first off-shore wind project with a capacity of 30 Megawatts was completed in the coast of Rhode Island, and the U.S. offshore wind project development pipeline includes over 20 projects totaling over 24 Gigawatts potential capacity [3].

Nevertheless, wind turbines have certain shortcomings. One of the biggest disadvantages of wind power is its inconsistency. Wind speed and direction fluctuates everyday and thus by itself cannot provide reliable power. A common strategy to solve this problem is the integration of energy storage, such as compressed air energy storage, so that it would store the energy during the times that the electricity production exceeds the electrical demand, as in off-peak hours or high wind conditions, and would return the stored energy back to the system when the turbine cannot meet the electrical demand. To mitigate this problem, in addition, the best location is selected before installing wind turbine to make sure it has the sufficient supply of wind. Higher altitudes and off-shore locations experience higher speeds and better consistency of

wind which makes these locations more desirable. However, with higher altitudes and off-shore locations comes bigger, more complex, and more expensive foundations. According to [4], over 26% of the cost of a 5MW turbine is its tower, and thus any development in lowering the turbine weight can substantially affect the turbine cost.

1.2 Wind Turbine Technology

Wind turbines are devices that convert the kinetic energy of wind to electrical energy. Wind mills are one of the oldest use of wind power ever existed which dates back to 500-900 AD. However it wasn't until 1888 that first wind powered electricity was built by Charles Brush. Nowadays, wind turbines are manufactured in wide range of types and sizes for uses in applications ranging from small scale such as RVs and boats, to medium scale such as domestic power supply and selling electricity to grid, to large utility scale such as wind farms.

Wind turbines are generally categorized into two configurations of horizontal axis and vertical axis. However, as a result of efficiency advantage of horizontal axis turbines, they are favored for utility scale implementations, and will be the focus of discussion in this paper. Wind turbines consist of various components. In conventional wind turbines, a shaft connects the blades and rotor to the generator located inside the wind turbine housing, known as nacelle. Large wind turbines rotate with relatively low speed of 30-60 rpm due to high inertia. However, most generators need at least 15 times of that speed to produce electricity [5]. Therefore, a gearbox is needed to do the required speed conversion. Gearboxes are heavy and costly and make up about 13% of the total cost of a wind turbine [4].Therefore any configuration that can eliminate the need for a gearbox can substantially lower the initial and maintenance costs.

Three important data that are used for the control and optimization of the wind turbine operation are wind speed, rotor speed, and wind direction. These are gathered by the anemometer, reed sensor, and wind vane, respectively, which then is processed

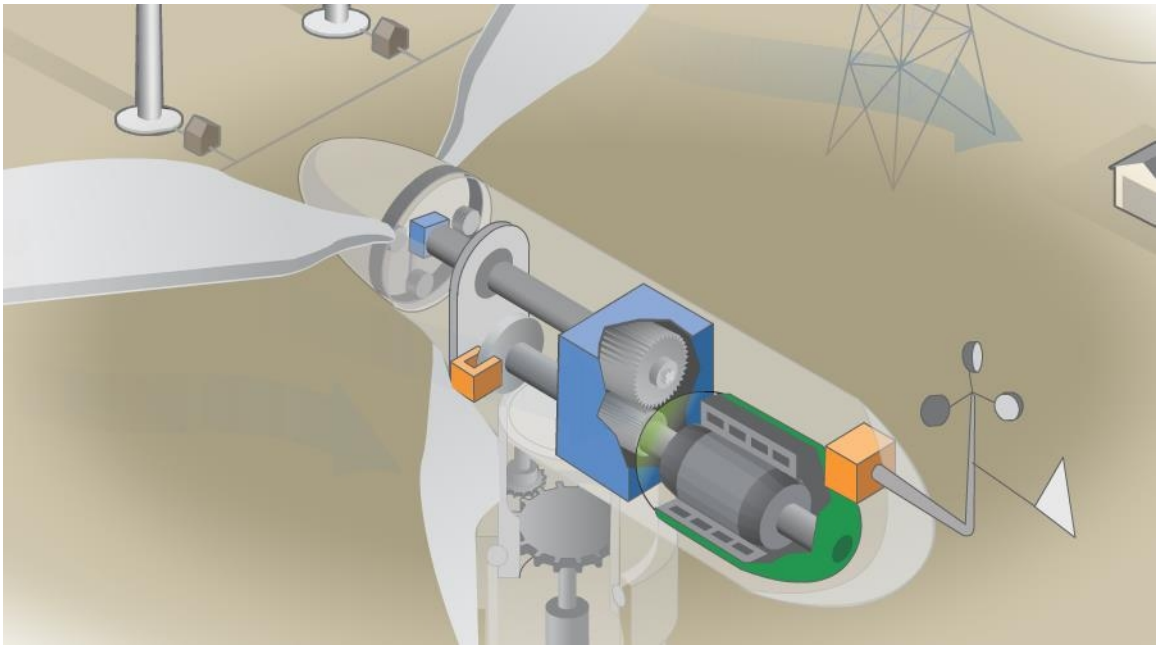

Fig. 1.2. Schematic of the internal components of wind turbine [3]

by the control unit. The control unit then adjusts the wind turbine direction, known as yaw, or changes the turbine blade angle, known as pitch angle, or controls the generator rotational speed, or shuts off the wind turbine at very high wind speeds to prevent damage to the internal components.

Wind power is the kinetic energy per unit time of wind, which depends on the mass flow rate and the speed of the wind. Therefore, we have:

$$P_{wind} = \frac{1}{2}\dot{m}V_{wind}^2 = \frac{1}{2}\rho A V_{wind}^3 \tag{1.1}$$

where P_{wind} is the power available in wind, ρ is the density of wind, A is the swept area of rotor, and V_{wind} is the wind speed. However, the power extracted by the wind turbine is not the full power available in wind, since the wind speed after the wind turbine would drop to zero. According to the Betz's law, the maximum theoretical efficiency a wind turbine can obtain is 59.3%. Therefore we have:

$$P_{rotor} = \frac{1}{2}\rho A V_{wind}^3 C_p(\lambda, \beta) \tag{1.2}$$

where $C_p(\lambda)$ is the power coefficient of the wind turbine that depends on the tip speed ratio, λ, which is defined as:

$$\lambda = \frac{R\omega_r}{V_{wind}} \tag{1.3}$$

where R is the radius of wind turbine rotor in meters, ω_r is the rotational speed of the wind turbine rotor in rad/s, and V_{wind} is in m/s. Power coefficient varies slightly with each turbine manufacturer and blade aerodynamic; however, generally their graphs follow similar pattern. A general equation for a power coefficient of a wind turbine can be expressed as [12]:

$$C_p(\lambda, \beta) = c_1(c_2\gamma - c_3\beta - c_4)e^{-c_5\gamma} + c_6\lambda \tag{1.4}$$

where

$$\gamma = \frac{1}{\lambda + 0.08\beta} - \frac{0.035}{\beta^3 + 1} \quad ,$$

β is the blade pitch angle, and c_1 through c_6 are constants, specific for each wind turbine. One of the important power quality factors of the generated power in wind turbines is the consistency of the frequency of the generated power. This will ensure that the generated electricity has the same frequency to penetrate the electricity grid in case of on-grid wind turbines, or be compatible and not to damage the equipment that are made to work with grid frequency, in case of off-grid wind turbine. This depends on the generator speed, and since the generator is connected to the hydraulic motor, controlling the rotational speed of the hydraulic motor would be the most efficient way to keep the generator frequency consistent. Therefore, an appropriate controller is needed to be designed to keep the motor at the same speed during the fluctuations in the wind.

1.3 Hydraulic Wind Power Transfer System (HWPTS)

As mentioned above, there are some shortcomings with the conventional wind turbines. As a result of significant research and improvements in the design and performance of wind turbines in the past decade, turbines with higher capacity have

been designed and installed which require reaching higher altitudes to operate. A gearbox is needed for each wind turbine, which is costly and adds weight to the wind turbine. This additional weight, thus, results in a bigger tower and foundation to support. Furthermore, the cost of having a separate generator for each wind turbine results in a higher payback period for wind farm projects.

Recent developments in implementing hydraulic drivetrains has shown to be competitive to conventional wind turbine structure [6]. In this configuration, the need for a gearbox is eliminated, and a hydraulic pump replaces the generator in the wind turbine nacelle by transferring the generator to ground level and allowing the hydraulic fluid to transfer the wind power to a hydraulic motor coupled to a generator. In doing so, multiple wind turbines can also be connected to feed the central generator. Since the wind turbines generate a large amount of torque at a relatively low angular velocity, a large displacement hydraulic pump is required. In tangent to the main generator, an auxiliary generator can also be implemented to allow the excess energy of the hydraulic fluid to be stored. In addition, ability of varying the pump and motor displacement allows for versatile operation modes for this system. Figure 1.3 demonstrates the schematic of a configuration of hydraulic wind power transfer system. As it can be seen, the rotor is mechanically coupled to a hydraulic pump that delivers the pressurized hydraulic fluid to the hydraulic motors coupled to generators in the ground level.

1.4 Energy Storage for the Wind Power Applications

One of the biggest disadvantages of the renewable energy resources is their intermittent nature. The reason is that we don't have control on the source of energy, as we do on the fossil fuels such as in coal power plants. This poses a challenge on full reliability on renewable energy sources and on the path to full independence from fossil fuels. One of the solutions to this issue is benefiting from energy storage. Energy storage devices can store energy when the power production is higher than

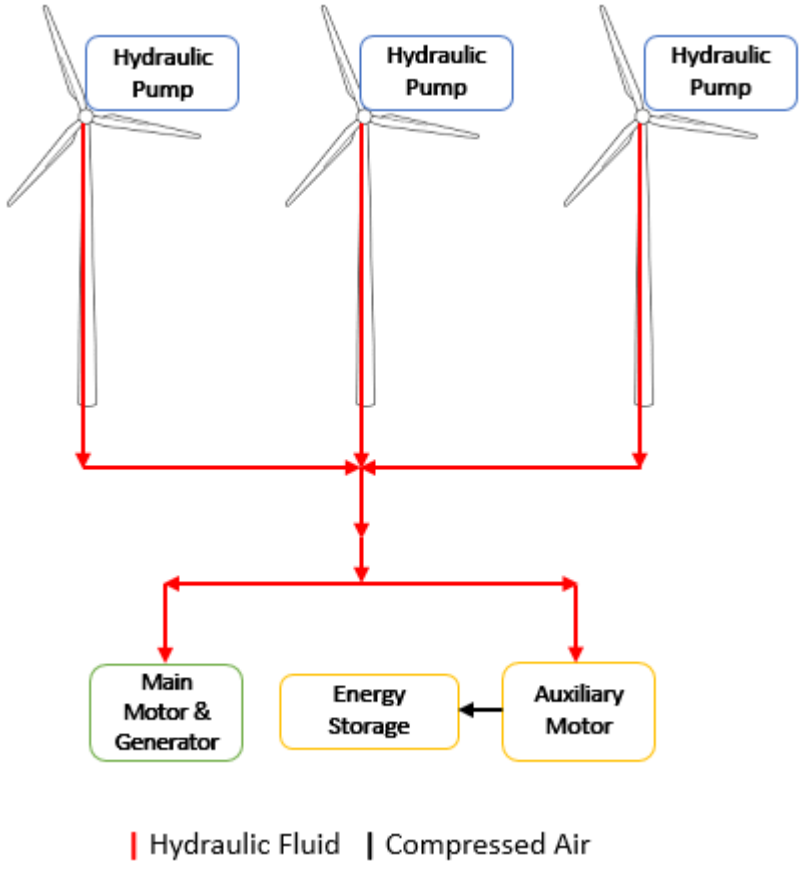

Fig. 1.3. Schematic of the Hydraulic Wind Power Transfer System (HWPTS)

the demand, and return it back when the produced power can't meet the demand. This can assist the renewable energy sources to meet the demand during periods of power shortage such as low winds or peak hours, and save energy during periods of unneeded power such as high winds or off-peak hours. There are numerous mediums and methods of energy storage that have been developed in the past century, which can be classified into mechanical, such as compressed air and pumped hydro, electrical, such as capacitors and super capacitor, electrochemical, such as rechargeable batteries, and thermal, such as hot rocks or concrete.

Compressed Air Energy Storage (CAES) is one of the only few technologies capable of storing and providing large utility-scale power and energy (above 100MW in single unit). It is also one of the most cost effective method of storing energy [9].

CAES takes advantage of the elasticity of air to increase its potential energy by increasing its pressure and releasing it when needed to generate electricity by directing the pressurized air to gas turbines. During the process, the air is compressed from atmospheric pressure to a pressure about 70 bar inside the storage tank. This air compression results in temperature increase, which must be rejected to be able to store the air efficiently in storage tanks. Heat exchangers, such as shell and tube, can be used for this purpose. During the expansion phase or discharge mode, in order to increase the output and the efficiency of the expansion train, the high-pressure air is heated either in combustors using natural gas or using the recovered heat from the compression stage. In order to recover the heat from compression stage for use in expansion stage, a Thermal Energy Storage (TES) is required between the compression and expansion stage. This configuration is known as Adiabatic-CAES (A-CAES), since no external heat or energy is added to the system during the process. The main components of the A-CAES system are: (1) Compression Train, (2) TES, (3) Air Storage Cavern, (4) Expansion Stage, (5) Motor/Generator.

The world's first CAES is the Germany's 290 MW Huntorf power plant, which was commissioned in 1978. This plant provides black-start power to nuclear units, back-up power to local power systems, and extra electrical power to fill the gap between the electricity generation and demand [8]. Another available CAES plant is the 110 MW Mcintosh power plant in Alabama, which was commissioned in 1991. This plant takes advantage of a recuperator that reuses the heat from the compression that increases the efficiency by about 10% [9]. However, they are currently no commissioned A-CAES plants. The efficiency of the current CAES plants are approximately 54% with the use of a recuperator. However, by installing TES, the need for natural gas combustion to heat the decompressed air is eliminated and thus the efficiency is raised to about 70% [10]. However, this technology comes with even more design and engineering challenges. The material, size and the shape of the TES must be engineered specifically according to the plant size and location to be able to provide adequate heat to the expanded air. Compression train also requires to be redesigned in

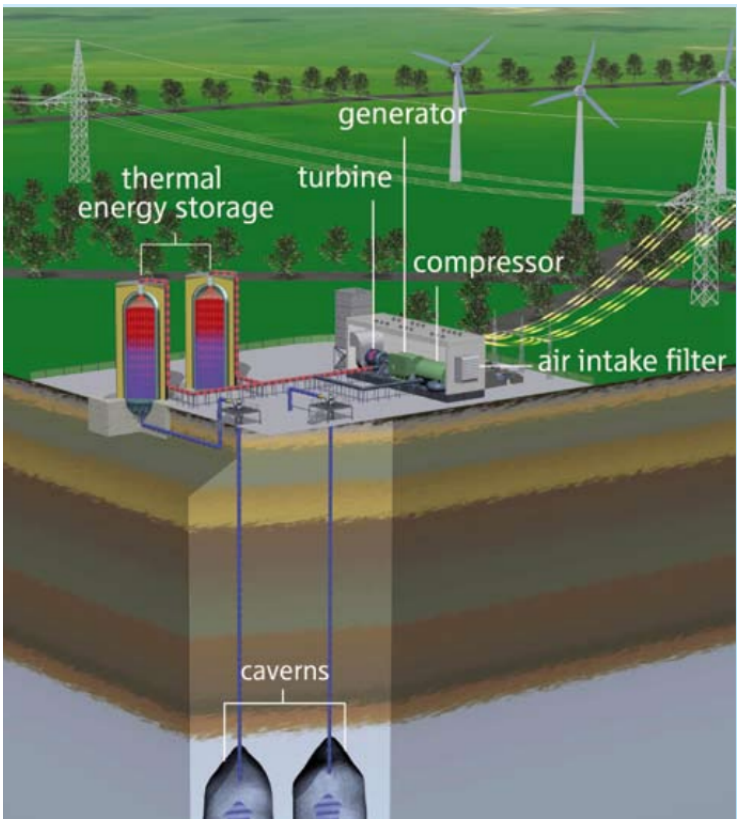

Fig. 1.4. Schematic of the Adiabatic Compressed Air Energy Storage [7]

order to extract the heat to the TES. Being zero-emission solution, academic interest and research has grown rapidly in this area, and there are currently few companies that are planning A-CAES systems around the world.

2. MODELING OF THE HYDRAULIC WIND POWER TRANSFER SYSTEM

Since the technology of Hydraulic Wind Power Transfer System (HWPTS) is still in research phase, a model of the system is important to study the effects of different variables in the system. In this chapter, we will discuss the governing equations and a state-space model of this technology, with the configuration of two wind turbines with a fixed-displacement pump located at each of them, directing a pressurized fluid to a fixed-displacement main and variable-displacement auxiliary hydraulic motors in the downstream. Note that this model can be also extended to more than two turbines. As shown in Figure 2.1, a small-scale prototype of this system is also built in Dr.Izadian's Energy System and Power Electronics Lab (ESPEL) to validate the governing equations of the system, which includes two electric motors representing two wind turbines that drive a pump directing the pressurized fluid to two hydraulic motors in the downstream, as discussed in [11]. During this process, the data were gathered through dSpace and the equations and constant values were verified.

The model represented in this chapter is discussed in two sections to capture the physical phenomena occurring in the system. In the first section, we will investigate the aerodynamics of the modeled turbine and construct the relation between the wind speed and the rotational velocity of rotor. In the second section, we will discuss the governing equations of hydraulic fluid, pumps, and motors, and relate them to the equations in the first section. Finally, a state-space model of the whole system will be presented to better understand the most important variable in the operation of each component. An integrated configuration of the components must be considered to obtain a detailed governing equation. This should incorporate initial conditions into the solution and represent the interrelation of the system equations.

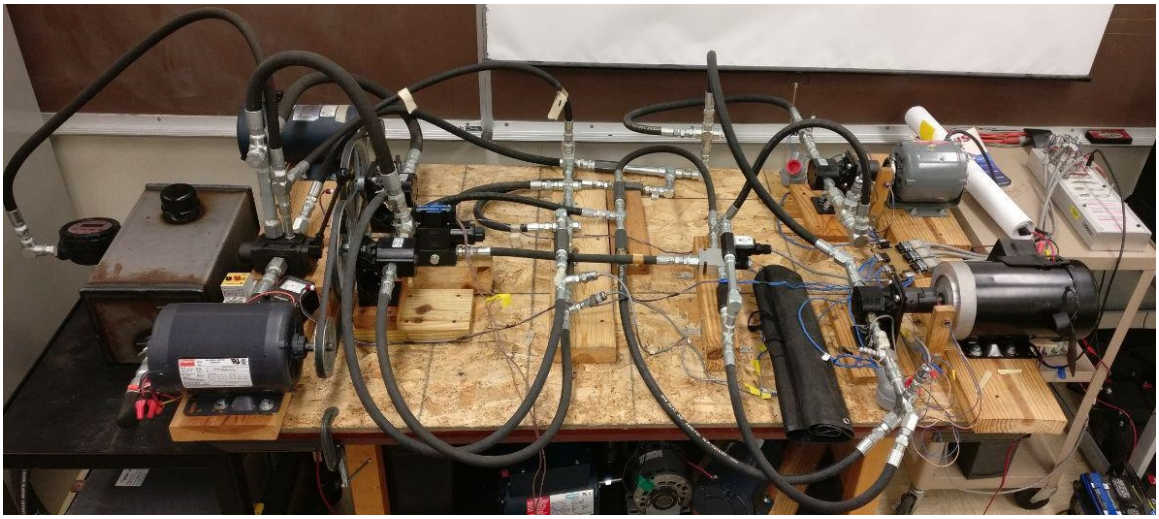

Fig. 2.1. Prototype of the Hydraulic Wind Power Transfer System, in Energy System and Power Electronics Lab (ESPEL)

2.1 Aerodynamic of the Wind Turbine

Wind turbines are in various sizes and blade shapes. Furthermore, wind turbine experiences a wide range of conditions during operation. This variability complicates the comparison of different turbines. The coefficient of power is the most important variable in aerodynamics of wind turbines. The power harvested by the wind turbine can be obtained by the following equation [12]:

$$P_{rotor} = \frac{1}{2}\rho A V_{wind}^3 C_p(\lambda, \theta) \tag{2.1}$$

where $C_p(\lambda, \theta)$ is obtained by:

$$C_p(\lambda, \theta) = c_1(c_2\gamma - c_3\theta - c_4)e^{-c_5\gamma} + c_6\lambda \tag{2.2}$$

in which γ is obtained by:

$$\gamma = \frac{1}{\lambda + 0.08\theta} - \frac{0.035}{\theta^3 + 1} \tag{2.3}$$

and $c_1 = 0.5176$, $c_2 = 116$, $c_3 = 0.4$, $c_4 = 5$, $c_5 = 21$, $c_6 = 0.0068$ [12], ρ is the density of air, A is the swept area of the wind turbine, V_{wind} is the effective wind speed

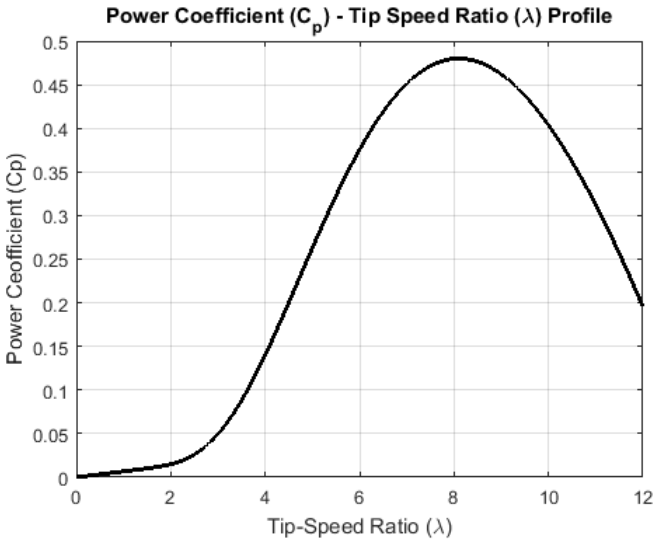

Fig. 2.2. Variation of power coefficient with respect to tip-speed ratio

through the wind turbine, β is the rotor's blade angle known as the pitch angle, and λ is the tip-speed ratio that can be obtained as:

$$\lambda = \frac{R\,\omega_{rotor}}{V_{wind}} \tag{2.4}$$

where $R = 28\,m$ is the radius of the wind turbine blade, ω_{rotor} is the rotational velocity of the rotor. Figure 2.2 shows the graph of the power coefficient C_p described in the equation (2.2) above. As it can be observed, there is an optimal tip-speed ratio for each wind turbine that harvests the maximum amount of energy from wind.

The exerted torque on the wind turbine shaft by the wind power can be obtained by the following equation:

$$\tau_{rotor} = \frac{P_{rotor}}{\omega_{rotor}} \tag{2.5}$$

2.2 Hydraulic Components

In hydraulic powertrain, the two wind turbine rotor shafts are mechanically coupled to the pumps that direct the pressurized fluid to two hydraulic motors in the downstream. The flow that is delivered by each pump is determined by:

$$Q_p = D_p \omega_p - k_{L,p} p_p \tag{2.6}$$

where D_p is the pump displacement, ω_p is the pump angular velocity which is same as ω_{rotor}, p_p is the pressure across pump, and $k_{L,p}$ is the pump leakage coefficient and is expressed as follows:

$$k_{L,p} = K_{HP,p}/\rho\nu \tag{2.7}$$

where ρ is the hydraulic fluid density, ν is the hydraulic fluid viscosity, and $K_{HP,p}$ is the pump Hagen–Poiseuille coefficient and is defined as [13]:

$$K_{HP,p} = \frac{D_p \omega_{nom,p}(1 - \eta_{vol,p})\nu_{nom}\rho_{nom}}{p_{nom,p}} \tag{2.8}$$

where $\omega_{nom,p}$ is the pump's nominal angular velocity, $\eta_{vol,p}$ is the pump volumetric efficiency, ν_{nom} is the nominal fluid kinetic viscosity, ρ_{num} is the nominal fluid density, and $p_{nom,p}$ is the nominal fluid pressure. Torque at the pump driving shaft is expressed by:

$$\tau_p = D_p p_p/\eta_{mech,p} \tag{2.9}$$

where $\eta_{mech,m}$ is the mechanical efficiency of the motor and is expressed by;

$$\eta_{mech,m} = \eta_{total,m}/\eta_{vol,m} \tag{2.10}$$

Therefore, the rotational acceleration of the pump can be expressed as the sum of the torques at the pump divided by the inertia of the rotor as:

$$\dot{\omega}_p = \frac{1}{J_{rotor}}(\tau_{rotor} - c_{v,p}\omega_p - c_{f,p}p_p - \tau_{b,p} - \tau_p) \tag{2.11}$$

where J_{rotor} is the moment of inertia of the rotor, $c_{v,p}$ and $c_{f,p}$ are the viscous drag coefficient and Coulomb friction coefficient, respectively, and $\tau_{b,p}$ is the breakaway torque of the pump shaft.

Hydraulic motors receive the flow supplied by the system and acts as a reverse pump. The flow supplied to the motor can be obtained as:

$$Q_m = D_m \omega_m + k_{L,m} p_m \tag{2.12}$$

where D_m is the motor displacement, ω_m is the motor's angular velocity, P_m is the pressure across motor, and $k_{L,m}$ is the motor's leakage coefficient, which is defined the same way as in equation (2.7). The torque at the motor driving shaft is expressed as:

$$\tau_m = D_m p_m \eta_{mech,m} \tag{2.13}$$

Therefore, the rotational acceleration of the motor can be expressed as the sum of the torques at the motor divided by the inertia of the motor shaft as:

$$\dot{\omega}_m = \frac{1}{J_{motor}} (\tau_m - c_{v,m}\omega_m - c_{f,m} p_m - \tau_{b,m} - \tau_L) \tag{2.14}$$

where J_{motor} is the moment of inertia of the motor shaft, $c_{v,m}$ and $c_{f,m}$ are the viscous drag coefficient and Coulomb friction coefficient, respectively, $\tau_{b,m}$ is the breakaway torque of the motor, and τ_L is the external load torque on motor shaft.

The compressibility equation represents the dynamics of the hydraulic hose and the hydraulic fluid. Based on the law of mass conservation and the definition of bulk modulus, the fluid compressibility within the system can be expressed as [14]:

$$\frac{dp}{dt} = \frac{\beta}{v} (\sum Q_p - \sum Q_m) \tag{2.15}$$

where β is the fluid bulk modulus and v is the fluid volume. If all the parts of the system are connected together, the pressure across the system will be same and thus, can just be expressed as p.

2.3 State-Space Representation

In previous section, the governing equations of the hydraulic components were provided to derive the state-space representation of the HWPTS. The key advantages

of the state-space representation comprise a detailed mathematical demonstration of the system that incorporates the initial conditions into the solution. The overall hydraulic system can be connected as modules to represent the dynamic behavior. The model incorporates the mathematical governing equations of individual hydraulic circuit components. The governing equations that are used to form the state-space representation can be summarized as:

- **Turbine Aerodynamics:** Equations (2.1) (2.2) (2.3) (2.4) (2.5)
- **Hydraulic Pump:** Equations (2.6) (2.7) (2.8) (2.9) (2.10) (2.11)
- **Hydraulic Motor:** Equations (2.12) (2.13) (2.14)
- **Hydraulic Pressure:** Equation (2.15)

A general form of a state-space model can be written as:

$$\begin{aligned} \dot{\mathbf{x}}(t) &= \mathbf{f}(t, x(t), u(t)) \\ \mathbf{y}(t) &= \mathbf{h}(t, x(t), u(t)) \end{aligned} \tag{2.16}$$

For modeling the HWPTS, the state variables are ω_{p1}, ω_{p2}, ω_{m1}, ω_{m2}, and p, which are the rotational speed of turbine 1, turbine 2, motor 1 (main), motor 2 (auxiliary), and the system pressure, respectively. Based on the values provided in the Table 2.1 for the constants used in the equations above, we obtain the following state-space representation:

$$\begin{pmatrix} \dot{\omega}_{p1} \\ \dot{\omega}_{p2} \\ \dot{\omega}_{m1} \\ \dot{\omega}_{m2} \\ \dot{p} \end{pmatrix} = \begin{pmatrix} (\tau_{rotor1} - 1012.23\,\omega_{p1} - 0.000169\,p)/1320000 \\ (\tau_{rotor2} - 1012.23\,\omega_{p2} - 0.000169\,p)/1320000 \\ (0.001\,p - 1.7475212\,\omega_{m1} - 0.00000358\,p - \tau_{L1})/80 \\ (D_{m2}\,p - 1.7475212\,\omega_{m2} - 0.00000358\,p - \tau_{L2})/80 \\ (Q_{p1} + Q_{p2} - Q_{m1} - Q_{m2}) \times 45.8333 \times 10^9 \end{pmatrix} \tag{2.17}$$

In the above representation, the value for D_{m2} was not included since it is a variable displacement motor, and will be used as control input. In addition, the values of T_{L1} and T_{L2}, which represent the load torque on the motor shafts, are also control

Table 2.1.
Specifications of hydraulic components

Symbol	**Description**	**Value**	**Unit**
D_m	Main Motor Displacement	1,000	cc/rev
D_p	Pump displacement (both turbines)	50,000	cc/rev
$K_{s,p}$	Pump slippage coefficient	72	cc/bar
$K_{s,m}$	Motor slippage coefficient	135	cc/bar
$C_{v,p}$	Pump viscous drag coefficient	106	N.m/rpm
$C_{v,m}$	Motor viscous drag coefficient	0.183	N.m/rpm
$C_{f,p}$	Pump Coulomb friction coefficient	16.9	N.m/bar
$C_{f,m}$	Motor Coulomb friction coefficient	0.358	N.m/bar
τ_{bp}	Pump breakaway torque	360	N.m
τ_{bm}	Motor breakaway torque	20	N.m
J_{rotor}	Rotor/pump moment of inertia	1.32×10^6	$kg.m^2$
J_{motor}	motor moment of inertia	80	$kg.m^2$
β	Fluid bulk modulus	1.1×10^4	bar
v	Fluid volume of the system	240	Litre

inputs and will be determined by the control strategy. As can be seen from the above state-space representation, pressure variation plays the most important role in system operation, since it is present in each row of the state-space representation. In addition if we consider the torque produced at the rotor side as whole as the input to the system, the system is bilinear, meaning that the only nonlinearity that exists in the system equations is the product of input and state variable, as in 4^{th} and 5^{th} row of the state-space equation. Otherwise, if we consider the wind speed as the input, due to the high nonlinearity of the power coefficient (C_p), as expressed in equation (2.2), our system would be nonlinear.

2.4 Model Results

The general dynamics of the system is generally governed by the five equations described in the state-space representation of equation 2.17. To demonstrate these equations and the behavior of the system, initial conditions need to be stated. It can be represented as a vector as follows:

$$x_0 = [\omega_{p1,0} \qquad \omega_{p2,0} \qquad \omega_{m1,0} \qquad \omega_{m2,0} \qquad p_0] \tag{2.18}$$

As can be observed from the equation 2.17, there are three inputs which are the displacement of the auxiliary motor, load torque of the main generator, and the load torque of the auxiliary generator as:

$$u = [D_{m2} \qquad \tau_{L1} \qquad \tau_{L2}] \tag{2.19}$$

Wind speed can be considered as en external input or disturbance which affects the torque of the turbine/pump shaft. Therefore the disturbances can be written as:

$$w = [\tau_{rotor1} \qquad \tau_{rotor2}] \tag{2.20}$$

For the purpose of simulation, a same wind speed is considered to be affecting the both turbines. All of the initial conditions of the equation 2.18 is also considered to be 0 at $t_0 = 0$. Figure 2.3 demonstrates the wind speed profile affecting the both turbines, which starts as 10 m/s at $t = 0s$, steps up to 13 m/s at $t = 200s$, and steps down to 8 m/s at $t = 400s$.

The resulting rotational speed profile of the turbine is shown in Figure 2.4. As can be noticed, the effect of the nonlinearity of the power coefficient (C_P) is shown in the first 200 seconds.

Figure 2.5 demonstrates the frequency of the main generator without any control systems installed. As can be observed, without an appropriate control strategy the frequency of the main generator does not stay constant.

Figure 2.6 demonstrates the rotational velocity of the auxiliary motor. This motor is designed to receive the excess fluid of the system. However, without appropriate

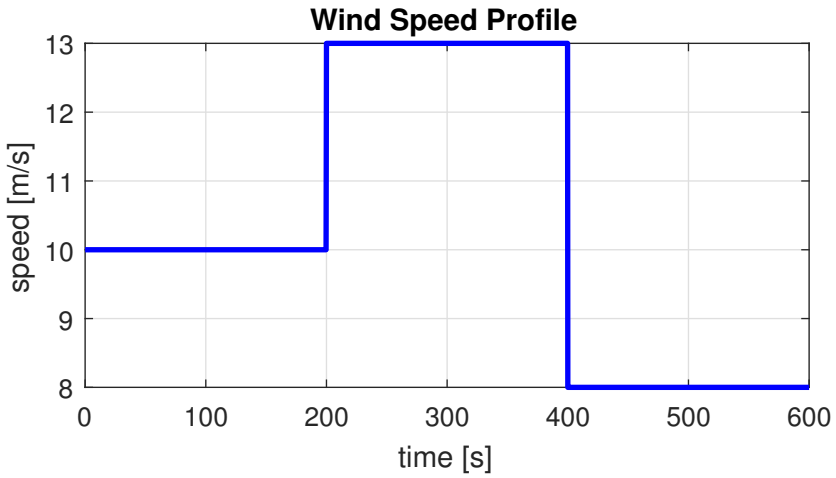

Fig. 2.3. Diagram of the control system for the compressed air energy storage

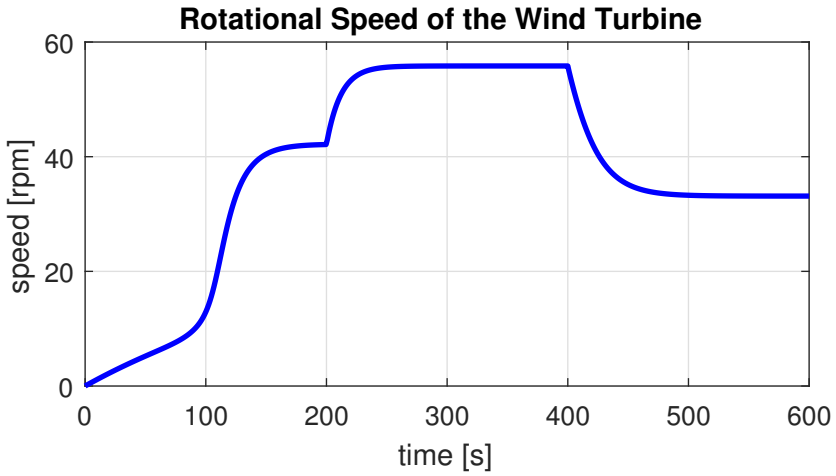

Fig. 2.4. Diagram of the control system for the compressed air energy storage

control strategy, the hydraulic fluid simply is distributed between main and auxiliary motors.

Figure 2.7 shows the pressure of the hydraulic fluid within the system. As can be seen, the effect of the nonlinearity of the power coefficient (C_P) can be observed between the $t = 0$ to 200 seconds.

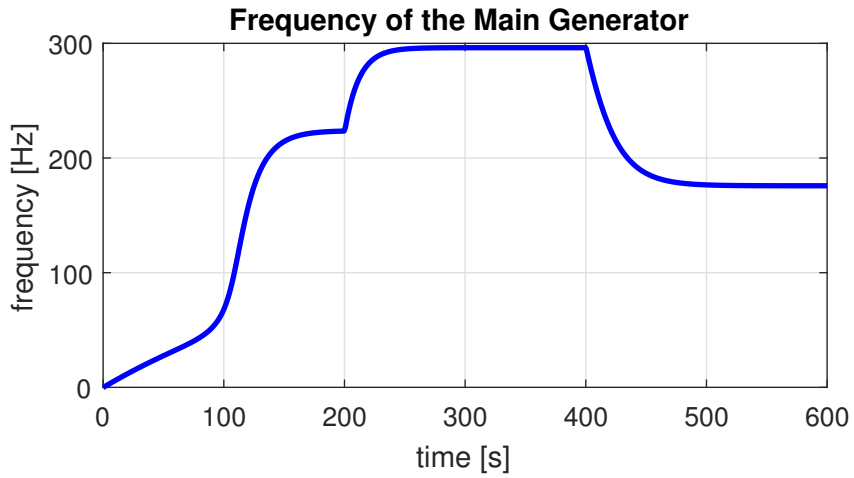

Fig. 2.5. Frequency of the main motor/generator shaft

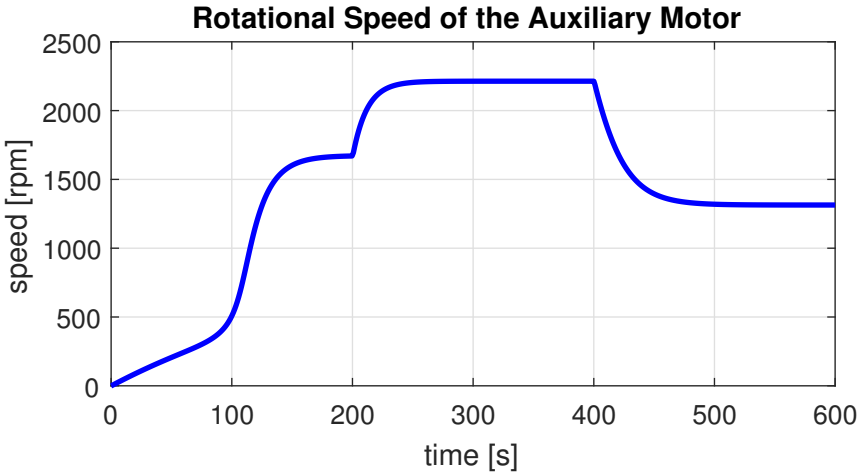

Fig. 2.6. Angular velocity of the auxiliary motor

Figure 2.8 shows the power coefficient of the wind turbine, which indicates the ability of the wind turbine in capturing the available wind power. Negative values of the power coefficient indicates the motoring operation [nrel].

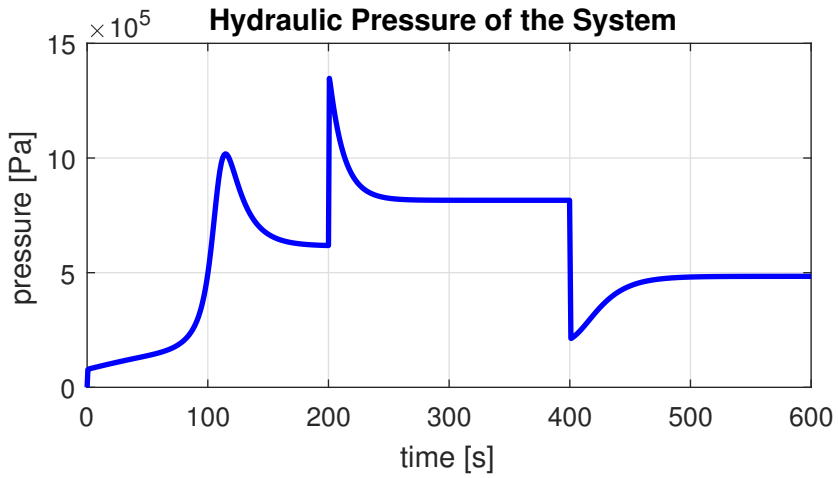

Fig. 2.7. Pressure of the hydraulic fluid within the system

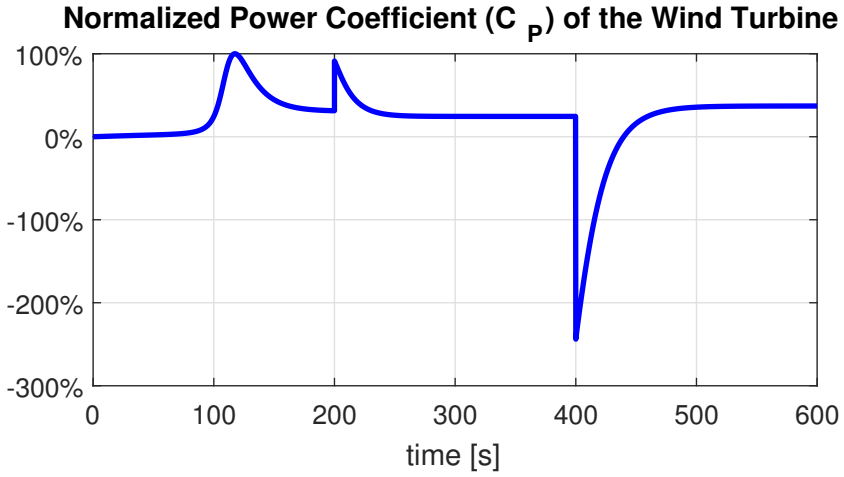

Fig. 2.8. Normalized Power Coefficient (C_P/C_{Pmax}) of the system

3. INTEGRATION OF ENERGY STORAGE

As discussed earlier, energy storage can mitigate the operation unreliability of wind turbines, especially in off-grid and microgrid applications. As demonstrated in Figure 1.3, energy storage can be coupled to Hydraulic Wind Power Transfer System (HWPTS) through the auxiliary motor. There are several energy storage technologies that can be integrated with the HWPTS, such as Compressed Air Energy Storage (CAES), Pumped Hydro Storage (PHS), flywheel, batteries, etc., and each one have their own advantages and disadvantages. According to [9], CAES is one of the cost-effective and one of the only few technologies suitable for large-scale utility applications. In this chapter, we will be discussing the governing equations of CAES and its integration with the HWPTS.

3.1 Modeling of the Compressed Air Energy Storage (CAES)

CAES operates based on the air elasticity and compressibility. Surplus power is stored inside the air storage cavern as pressurized air during the periods when the wind power is higher than the electricity demand, such as in off-peak hours or high wind hours, and is discharged from the cavern when wind turbine can't meet the electricity demand, such as in peak hours or low wind hours. Main components of the CAES are: Compression Train, Heat Exchangers, Air Storage, and Expansion Train. In this section we will be discussing the governing equations of the CAES.

3.1.1 Compression Stage

The multi-stage air compression unit consists of a group of Low Pressure (LP) and High Pressure (HP) compressors. Based on the mass balance of the compression

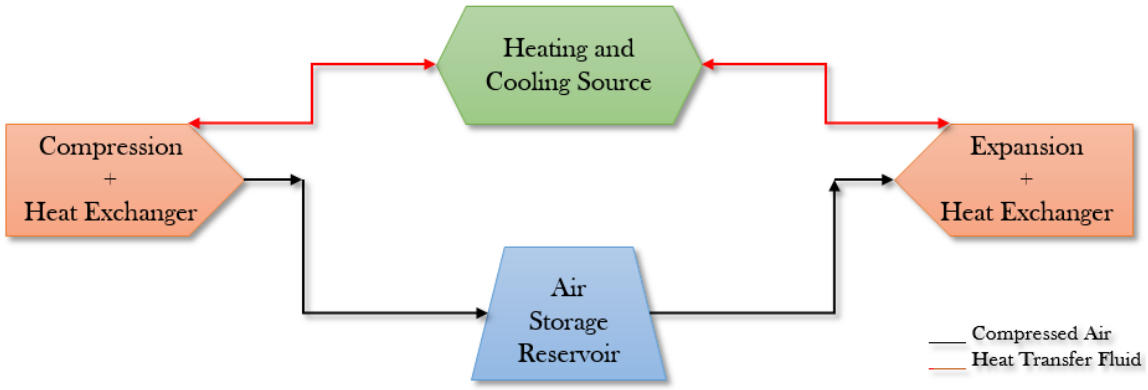

Fig. 3.1. Schematic of the Compressed Air Energy Storage (CAES)

process, the input mass flow rate of the compression train is proportional to the available surplus power. Temperature of air rises rapidly as a result of compression, which is inefficient for compression process, and thus, heat exchanger coils are incorporated between compressors and before air storage reservoir to reduce the temperature of the compressed air. The pressure of the air that passes through a compressor increases as following:

$$p_{c,a}^{out} = p_{c,a}^{in}\,\beta_c \tag{3.1}$$

where p is the pressure, β is the compression ratio, and subscripts c, a, out, and in refer to compressor, air, outlet, and inlet, respectively. When there is a steady flow of fluid in and out of a thermodynamic system, from the first law of thermodynamics we have:

$$\dot{m}_{in}\left(h_{in} + \frac{C_{in}^2}{2} + Z_{in}g\right) + \dot{Q} + \dot{W} = \dot{m}_{out}\left(h_{out} + \frac{C_{out}^2}{2} + Z_{out}g\right) \tag{3.2}$$

where $\dot{m}$ is the mass flow rate, h is the specific enthalpy, C is the fluid velocity, Z is the height of the system, $\dot{Q}$ is the rate of change of heat transferred, and $\dot{W}$ is the rate of change in energy transfer because of work done. By assuming that the air is an ideal gas, we have:

$$pv = mRT \tag{3.3}$$

where p is air pressure, V is the volume of air, m is the mass of the air, $R = 286.7\, J/kg.K$ is the universal gas constant, and T is the temperature of air. Considering the air expansion and compression to be a polytropic process, we would have:

$$pV^n = constant \tag{3.4}$$

As a result of the equations above we obtain the following equation, relating the temperature at the outlet and the inlet of the compressor [15]:

$$T_{c,a}^{out} = \beta_c^{(n_c-1)/n_c} T_{c,a}^{in} \tag{3.5}$$

where $T_{c,a}^{out}$ is the outlet air temperature of the compressor, $T_{c,a}^{in}$ is the inlet air temperature of the compressor, and n_c is the polytropic index of the compressor. Power consumed by each compressor is obtained as [15] [16]:

$$P_c = \frac{1}{\eta_c} \dot{m}_{c,a} c_{p,a} T_{c,a}^{in} \left(\beta_c^{(n_c-1)/n_c} - 1 \right) \tag{3.6}$$

In the above equation, η_c is the efficiency of the compressor, $\dot{m}_{c,a}$ is the air mass flow to the compressor, and $c_{p,a}$ is the specific heat capacity of air. After each compressor, a heat exchanger is placed to reduce the temperature of the air before entering the next compressor and before entering the air storage reservoir. A heat transfer fluid flows through the heat exchangers that alter the temperature of the incoming air. The temperature of the air at the outlet of the heat exchanger can be written as:

$$T_{HX,a}^{out} = T_{HX,a}^{in} + \eta_{HX} \left(T_{HX,HTF}^{in} - T_{HX,a}^{in} \right) \tag{3.7}$$

where $T_{HX,a}^{out}$ is the temperature of air at the outlet of the heat exchanger, $T_{HX,a}^{in}$ is the temperature of air at the inlet of the heat exchanger, η_{HX} is the efficiency of the heat exchanger, and $T_{HX,HTF}^{in}$ is the temperature of the incoming heat transfer fluid through the heat exchanger.

To find the required mass flow rate of the heat transfer fluid, we would need to find its energy balance with the incoming air. Therefore, we have:

$$\dot{m}_{c,HTF} = \frac{(T_{HX,a}^{out} - T_{HX,a}^{in}) c_{p,a} \dot{m}_{c,a}}{(T_{HX,HTF}^{in} - T_{HX,HTF}^{out}) c_{p,HTF}} \tag{3.8}$$

3.1.2 Air Storage

Depending on the size of the power plant, a manufactured or a natural geological formation can be utilized to store the compressed air. Manufactured storage reservoirs are usually used for smaller scale storage systems. They have better sealing, and thermal and insulation properties, but cost more. On the other hand, natural reservoirs are present in nature in very big sizes but they might not have the qualities of the manufactured storages.

As air enters and exits the reservoir, it changes the temperature and the pressure of the air in the storage. Ignoring the losses through the air storage wall, the temperature within the storage reservoir can be expressed as [15]:

$$\frac{dT_{s,a}}{dt} = \frac{1}{m_{s,a}}(1 - \frac{1}{k})(\dot{m}_{s,a}^{in} T_{s,a}^{in} - \dot{m}_{s,a}^{out} T_{s,a}^{out}) \tag{3.9}$$

where $T_{sc,a}$ is the air temperature within the air storage, $m_{sc,a}$ is the air mass at a given time inside the storage, $k = 1.4$ is the ratio of specific heat capacities of air, and subscripts *in* and *out* refer to the inlet and outlet of the air storage reservoir. $m_{sc,a}$ can be calculated at each step as:

$$\frac{dm_{s,a}}{dt} = \dot{m}_{s,a}^{in} - \dot{m}_{s,a}^{out} \tag{3.10}$$

3.1.3 Expansion Stage

This stage consists of several high pressure and low pressure turbines. In contrast to compression train, air needs to have a high temperature for efficient operation of turbine. Therefore, before entering the turbine, a heat exchanger is placed to reheat the air. The source of this heat can either be the recycled heat from the compression stage, that can be achieved using a carburetor or Thermal Energy Storage (TES), or external heat using combustion such as natural gas. Power produced by each turbine is expressed as [15]:

$$P_e = \eta_e \dot{m}_{e,a} c_{p,a} T_{e,a}^{in} (1 - \beta_e^{n_e - 1/n_e}) \tag{3.11}$$

where η_e is the efficiency of the turbine, $\dot{m}_{e,a}$ is the air mass flow through each turbine, $c_{p,a}$ specific heat of air, $T^{in}_{e,a}$ is the temperature of air at the inlet of turbine, β_e is the expansion ratio of each turbine, and $n_e = 1.1$ is the polytropic index of expansion. The mass flow rate of the heat transfer fluid can be found using the Equation (3.8). The pressure of the air after going through the turbine can be obtained as the inverse of the compression stage, which is:

$$p^{out}_{e,a} = \frac{p^{in}_{e,a}}{\beta_e} \tag{3.12}$$

where $p^{out}_{e,a}$ is the outlet pressure of the turbine and $p^{in}_{e,a}$ is the inlet pressure of the turbine. Similar to Equation (3.5), the temperature after the each turbine expansion stage can be found using the ideal gas law, and the assumption of polytropic process as [15]:

$$T^{out}_{e,a} = \beta_e^{(1-n_e)/n_e} T^{in}_{e,a} \tag{3.13}$$

Now that we have the governing equations of the CAES, the next step is to study the method of integrating the CAES with HWPTS.

3.2 Integration of CAES with HWPTS

Many of the current energy storage systems couple electrically with the power plant. To better understand, in a coal plant for example, coal is burnt to produce a mechanical energy that turns a generator to produce electricity, and afterwards, the excess electricity is used to run the energy storage system such as the CAES compressor. Conversion of mechanical energy to electricity and subsequently, converting the excess electricity to mechanical energy to be able to store reduces the efficiency of the system and causes losses during the conversion. Therefore to prevent conversion losses, a direct coupling method of CAES with HWPTS is proposed in this paper. In this method, the auxiliary hydraulic motor is coupled directly to the compressor shaft and provides the excess energy of the system to the compressor. During low-power times, energy of the stored air is used to rotate a turbine that drives a hydraulic

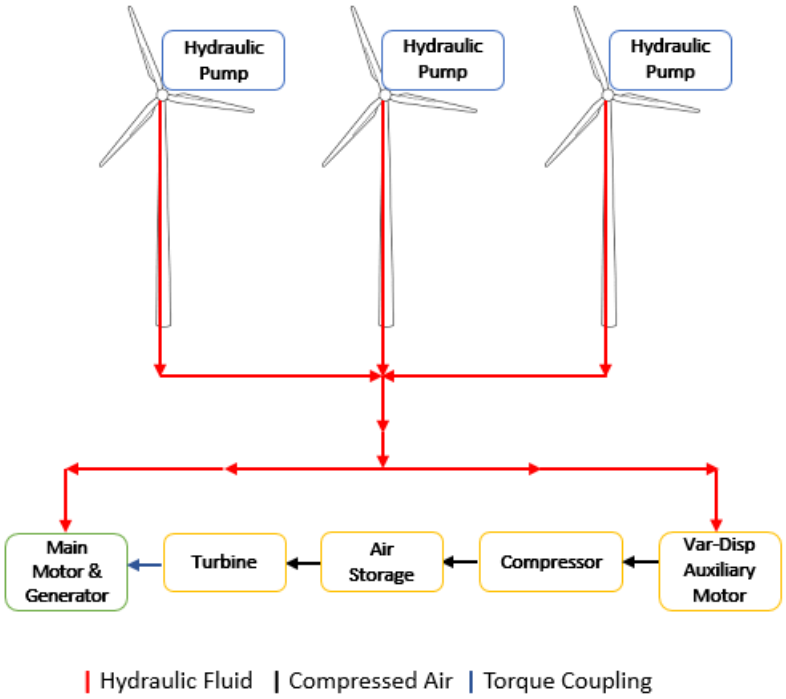

Fig. 3.2. Schematic of the integrated CAES with HWPTS

pump which provides pressurized hydraulic fluid to feed the main motor/generator at a required hydraulic flow rate.

As can be seen from the Figure 3.2, check valves are present in the system to provide a unidirectional flow in the required sections of the system. Open/close valve is present to control the operation of the auxiliary motor. It is closed during low-wind, when the CAES is discharging, in order to direct all of the flow to main motor/generator and prevent the charging of the CAES from auxiliary motor. It opens during high-wind operation in order to allow the excess flow to the auxiliary motor and charge the CAES.

3.2.1 CAES Sizing

Energy storage size consists of two factors which are power and energy. Power is the maximum power that a energy storage can provide, and energy is the amount

of the time that the energy storage is able to provide the maximum power. These factors can be calculated by analyzing the wind speed trends in the past for a specific location. By simulating the wind speed, the corresponding power obtained from the wind can be calculated. By setting the minimum power to the amount of power that is required to keep the main generator at the required frequency, we can obtain the longest duration in which the wind power was not able to meet the minimum power. Therefore, the power of the CAES can be chosen as the minimum power required to maintain the main generator at the required frequency, and the energy of the CAES can be chosen simulating the past wind data of a specific location, and calculating the required energy as the maximum power shortage period:

$$E_s = \max(\int_{t_1}^{t_2} \left(P_{main,min} - P_{main,wind}\right) dt) \tag{3.14}$$

where $P_{main,wind}$ is the power provided to the main generator by the wind, $P_{main,min}$ is the minimum power required to maintain the main generator at the required frequency, and t_1 to t_2 shows the durations in which the wind power was lower than the required main generator power.

4. CONTROL SYSTEM DESIGN

In order to achieve the best quality of power and maximize the efficiency of the turbine, certain factors need to be controlled and optimized. There are three factors that have been considered for this purpose: Keeping a constant frequency of the generated power, maximizing the power coefficient (C_p), and maximizing the output power of the generator. In the following sections, the control and optimization strategies along with the simulation results will be presented and discussed.

4.1 Frequency Control of the Main Motor

Previously, In order to control the frequency of main motor, a proportional valve was utilized to control the flow distribution to each motor [17]. However, this method causes energy loss due to pressure drop across the valve [18]. Thus, in order to eliminate the energy loss while controlling the frequency of the main motor, a variable-displacement auxiliary motor is introduced to the system to control the main generator frequency during sufficient wind power, and a CAES is integrated with the system to supply the required power during power shortage.

4.1.1 Frequency control using variable-displacement auxiliary motor

A variable-displacement motor is able to change its displacement volume. This causes changes to the hydraulic system pressure which affects the operation of the other components. Using this ability, we can suggest a method to control the rotational velocity of the main generator using the auxiliary motor. Using this method, not only the frequency of the main generator can be controlled, it will help reduce the power rating of the main motor and generator and provide an economic advan-

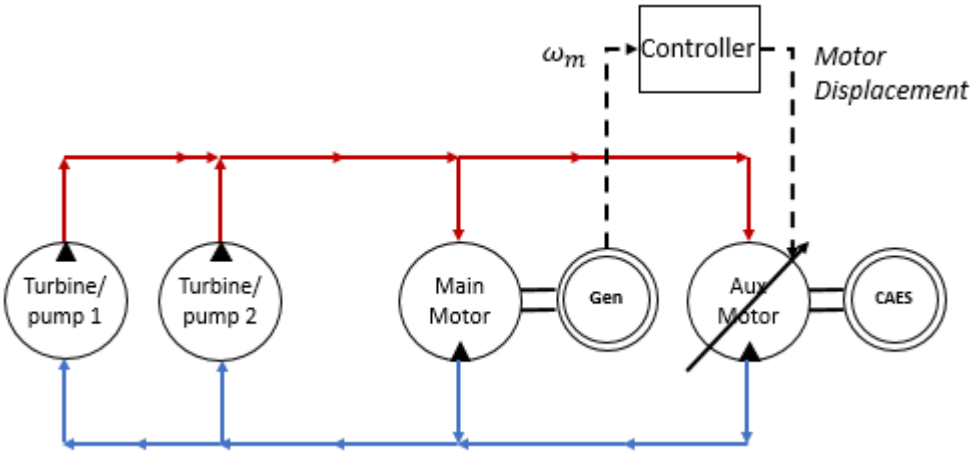

Fig. 4.1. Diagram of the control system for the optimization of Power Coefficient C_P

tage. This will allow an indirect control over the flow to the main motor. Thus, a control strategy for the auxiliary motor displacement (e.g. swashplate angle) needs to be developed. For this purpose, a PID controller is utilized to adjust the displacement based on the main motor's rotational velocity to keep it at a constant frequency. Proportional-Integral-Derivative controller (PID controller) is a control loop feedback mechanism widely used in variety of applications. PID controller continuously calculates the difference of the current value and the desired value known as the error, and applies proportional (k_p), integral (k_i), and derivative (k_d) values based on that. The term P is proportional to the current value of error $e(t)$. Meaning that if the difference of current and desired value is large, the control output will be proportionally large. The term I accounts for the past values of error and integrates them over time. The term D estimates the trend of the error value in the future based on the gradient of the error. Note that the term D can be eliminated in some cases from the controller. The control function of PID can be expressed as:

$$u(t) = k_p\, e(t) + k_i \int_0^t e(\tau)d\tau + k_d \frac{d}{dt} e(t) \tag{4.1}$$

In which $u(t)$ is the control signal. There are several methods to tune the controller gains to obtain the desired output. Some of the PID tuning methods are Ziegler-

Nicholas [19], Tyreus Luyben [20], etc. Ziegler-Nicholas method has proven to be effective and relatively easy method for tuning the parameters. Addressing the primary goal of the design makes the control system single input-single output (SISO). The controller output to the system is a position profile to the auxiliary motor sent by the designed controller in MATLAB/Simulink, and the primary output of the system is the speed of the main generator. Figure 4.2 is the diagram of the control system for this purpose.

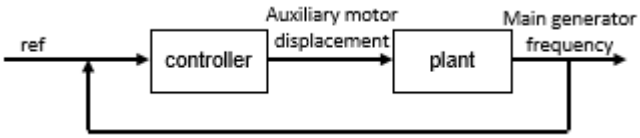

Fig. 4.2. Diagram of the control system for the variable-displacement auxiliary motor

For the simulation, the PID parameters are tuned manually by trial and error and familiarity to the system dynamic, and the resulting control law is obtained as:

$$D_{m2(aux)} = 5\left(\omega_{m,ref} - \omega_m(t)\right) + \int_0^{t_f}\left(\omega_{m,ref} - \omega_m(t)\right)dt \tag{4.2}$$

where $D_{m2(aux)}$ is the displacement of the auxiliary motor, $\omega_{m,ref}$ is the reference main generator rpm (frequency), and $\omega_m(t)$ is the current main generator rpm (fre-

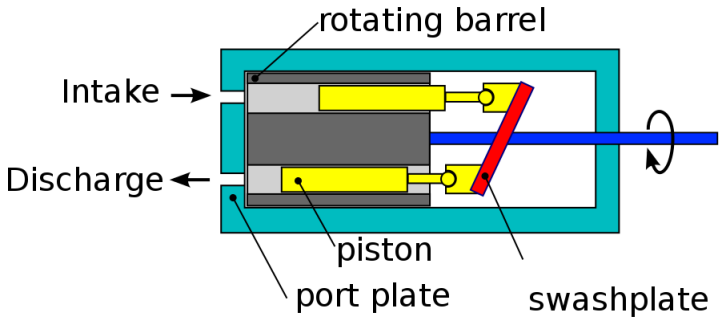

Fig. 4.3. Diagram of the control system for the compressed air energy storage

quency). This control circuit can be implemented in axial piston hydraulic motors, which have number of pistons in circular array within a cylindrical block. Figure 4.3 demonstrates the overall components of this type of motor. As can be noticed, by modifying the angle of the swashplate, one can change the displacement of the motor.

To verify the controller described, a simulation is conducted with the mentioned controller embedded. In this simulation, the controller receives the error signal of the main generator frequency, and calculates the output using a PI controller. The output of the controller is then sent to the auxiliary motor displacement. Figure 4.4 shows the wind speed profile that is used for the simulation.

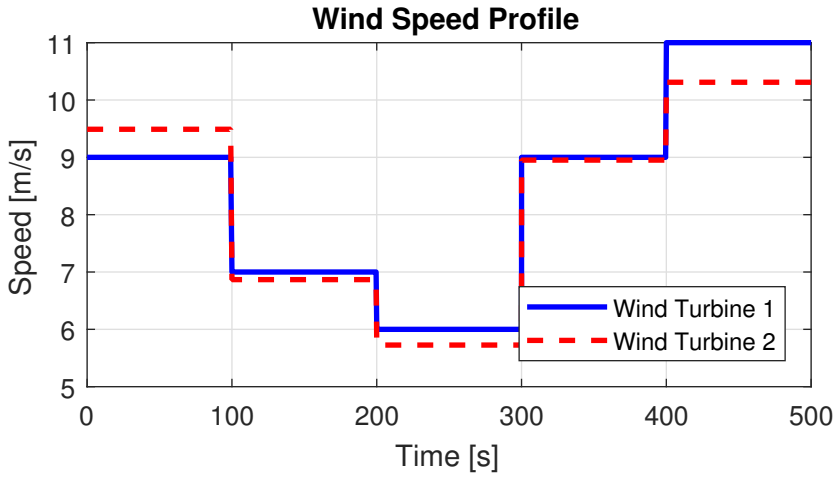

Fig. 4.4. Wind speed profile affecting the wind turbines

Figure 4.5 demonstrates the frequency of the main generator that is controlled. As can be seen the maximum variation occurs as soon as the controller is activated and the variation is about 0.07%.

Figure 4.6 shows the rotational speed of the wind turbines, which is directly affected by the wind speed and the hydraulic pressure variation within the system.

Figure 4.7 demonstrates the controller action, which is the displacement of the variable displacement auxiliary motor. The variation in the displacement of this motor alters the hydraulic pressure of the system which as a result, affects the operation of the other components.

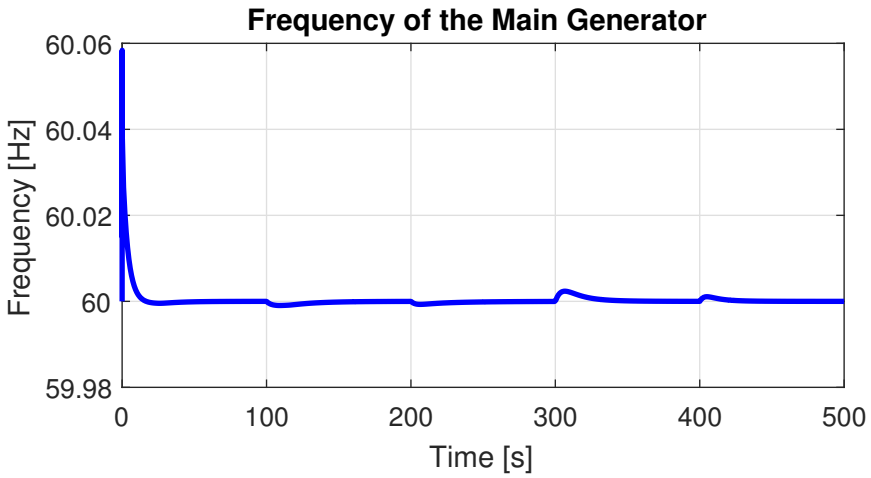

Fig. 4.5. Frequency of the main generator shaft

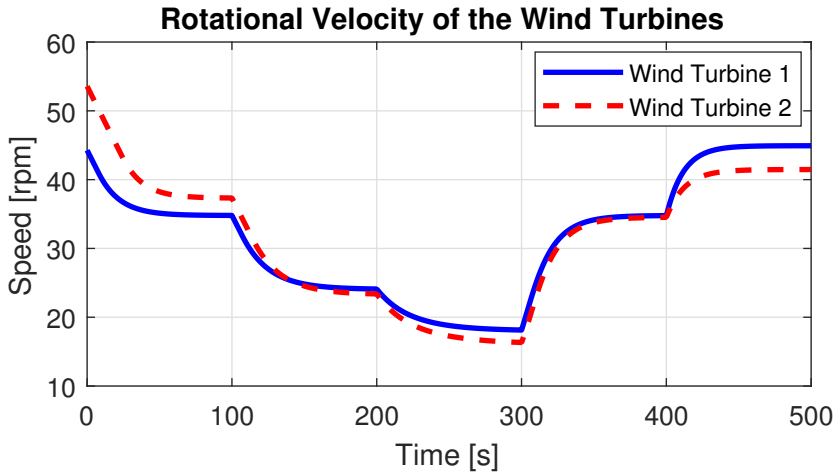

Fig. 4.6. Angular speed of the wind turbine shafts

Changes in the displacement of the auxiliary motor affects its rotational speed, which is described in Figure 4.8.

As described above, hydraulic pressure variation of the system affects the operation of the all other interconnected components. However, as can be observed in the figure 4.9, the pressure of the system is also kept constant as a result of the controller, since it directly affects the rotational speed of the main generator.

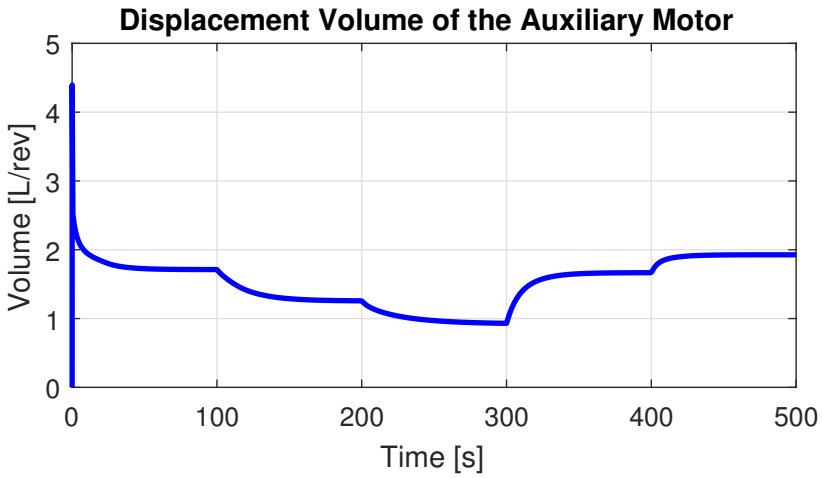

Fig. 4.7. Displacement variations of the variable-displacement auxiliary motor

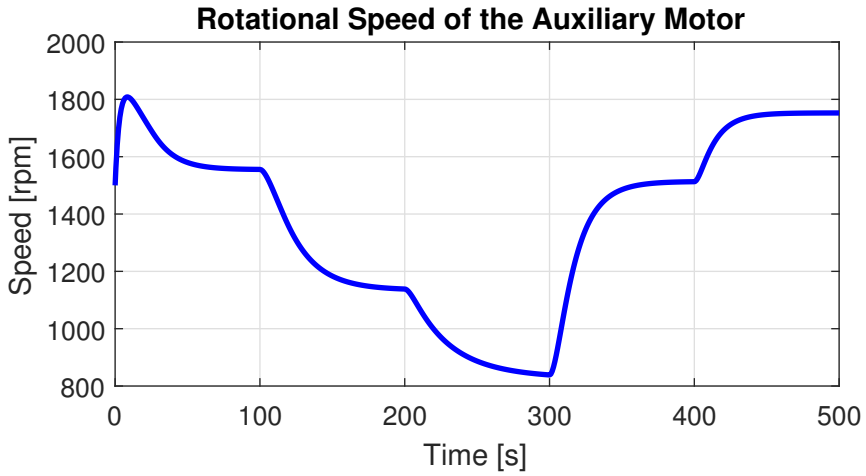

Fig. 4.8. Angular velocity of the auxiliary motor shaft

4.1.2 Frequency control using CAES

Compressed Air Energy Storage (CAES) is a technology to store energy for use at a later time using compressed air. It is one of the methods used for grid energy storage in utility scale, and is a well-known method for storing the generated electricity. During the process, the air is compressed from atmospheric pressure to storage pressure, and the air temperature is thus greatly increased. Multistage heat exchangers are used

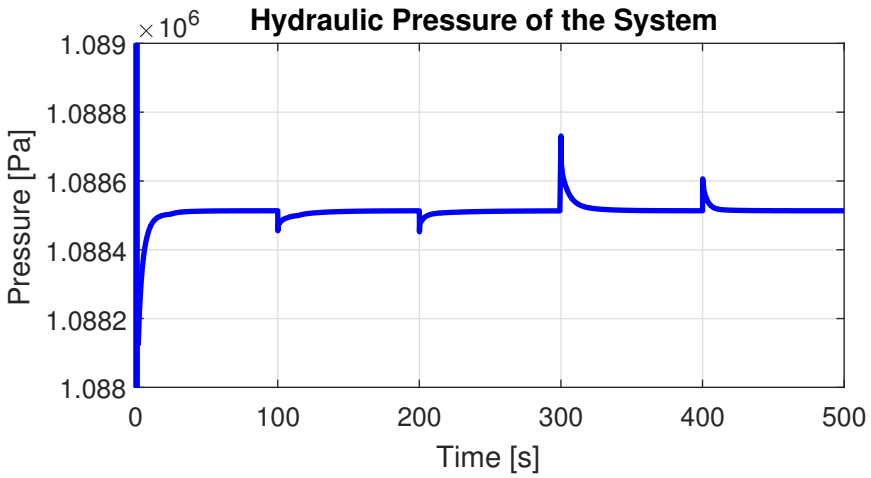

Fig. 4.9. Pressure of the hydraulic fluid within the system

to extract this heat before directing the air towards air storage tank. During the expansion phase, the high pressure air is heated in combustors either using natural gas, or using the extracted heat during compression phase for adiabatic expansion. In this stage, the expanded air is directed towards turbines. As discussed in Chapter 3, a hydraulic pump is connected to the turbine to provide the required pressurized hydraulic flow to the system.

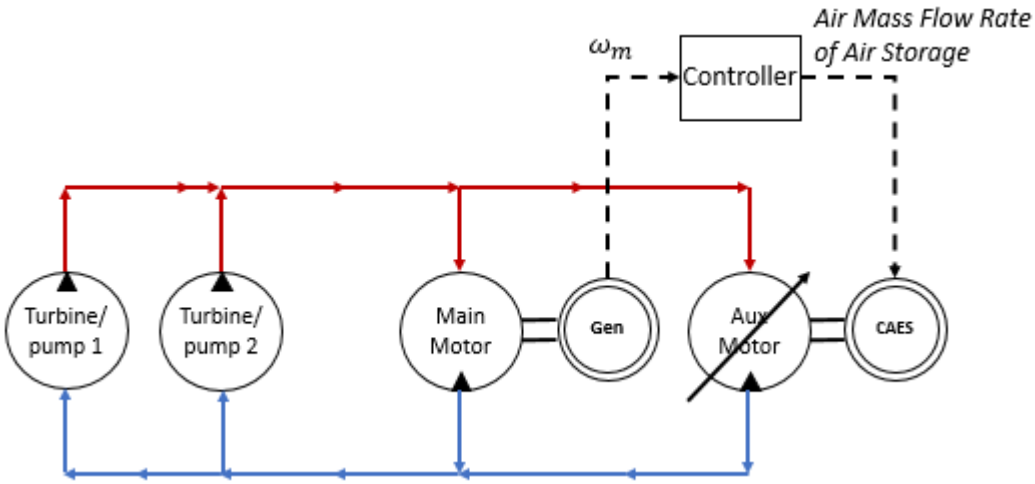

Fig. 4.10. Diagram of the control system for the frequency control using Compressed Air Energy Storage (CAES)

To control the amount of the air extracted from the air storage, a suitable control strategy is necessary. The input to this controller is the main generator frequency and the output is the air mass flow rate coming out of the air storage reservoir. For this purpose, a PID controller is tuned and utilized. Figure 4.11 is the diagram of the control system for this purpose.

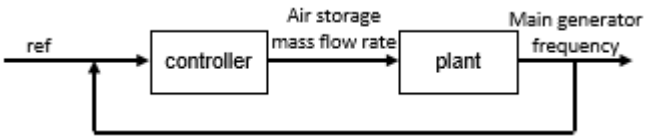

Fig. 4.11. Diagram of the control system for the compressed air energy storage

The PID parameters are tuned manually by trial and error and familiarity to the system dynamic, and the resulting control law to control the air mass flow rate of the CAES is obtained as:

$$\dot{m}_{e,a} = 10\left(\omega_{m,ref} - \omega_m(t)\right) + 3\int_0^{t_f}\left(\omega_{m,ref} - \omega_m(t)\right)dt \tag{4.3}$$

where $\dot{m}_{e,a}$ is the air mass flow rate of air storage towards the turbine, $\omega_{m,ref}$ is the reference rpm (frequency) of the main generator, $\omega_m(t)$ is the current rpm (frequency)

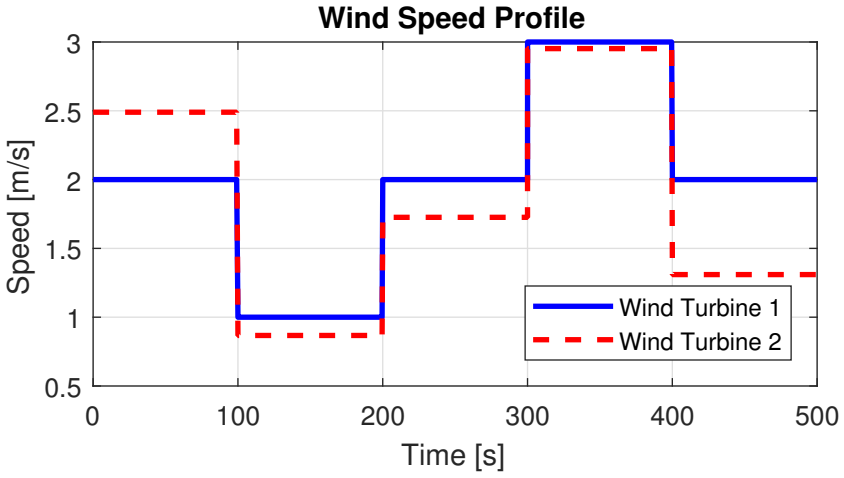

Fig. 4.12. Wind speed profile affecting the wind turbines

of the main generator. To test the described controller, the HWPTS is tested with this embedded controller. The wind speed profile needs to be slow so that it would not be able to provide the required power to the main generator. Therefore, the wind speed profile of the figure 4.12 is utilized.

Figure 4.13 shows the frequency of the main generator, which is kept constant at 60 Hz using the control system. The top part of the graph shows the all the graph and the bottom part provides a zoomed around the 60 Hz portion for any transients.

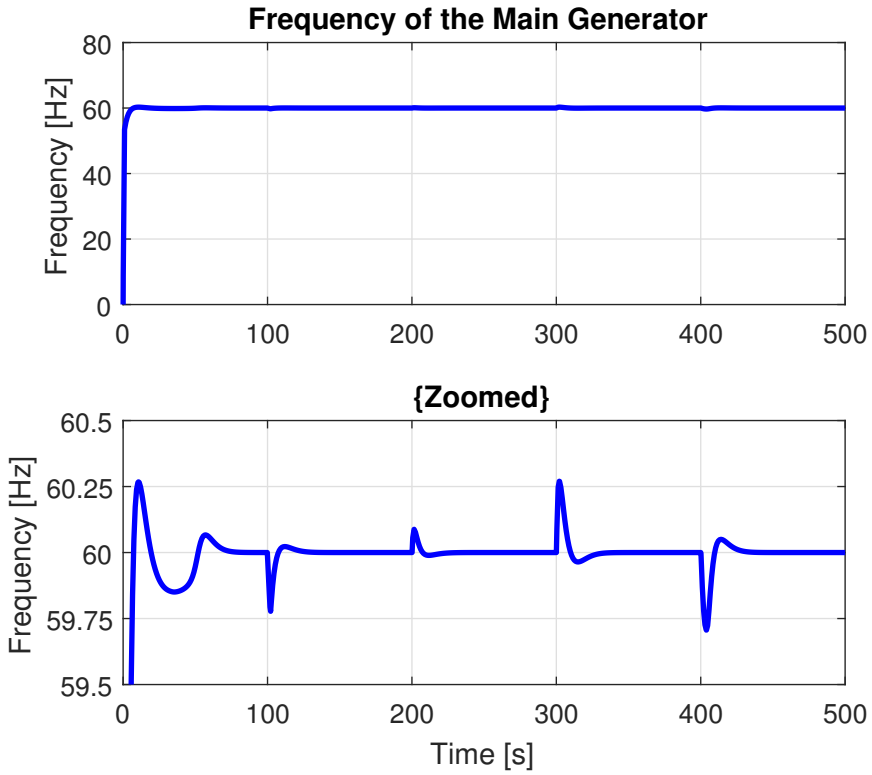

Fig. 4.13. Frequency of the main generator shaft

Figure 4.14 represents the rotational speed of the CAES turbine. The turbine is rotated by releasing the air from the air storage reservoir in order to provide the required power for the main generator's fixed frequency operation. The air is released

through an air valve and the position of the air valve is controlled based on the amount of the power that is needed from the air storage.

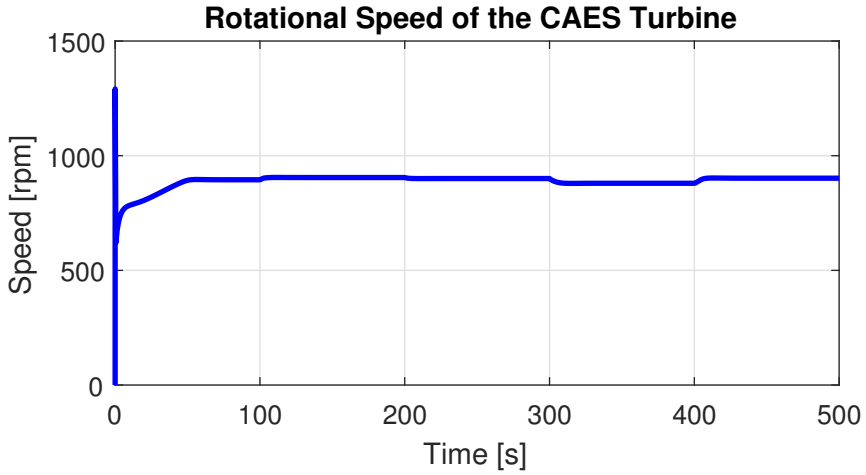

Fig. 4.14. Angular velocity of the turbine of the Compressed Air Energy Storage (CAES)

Figure 4.15 demonstrates the pressure variation inside the air storage reservoir. As can be observed, since the CAES is providing the required energy to run the main generator, the air is discharging, and thus the pressure is decreasing.

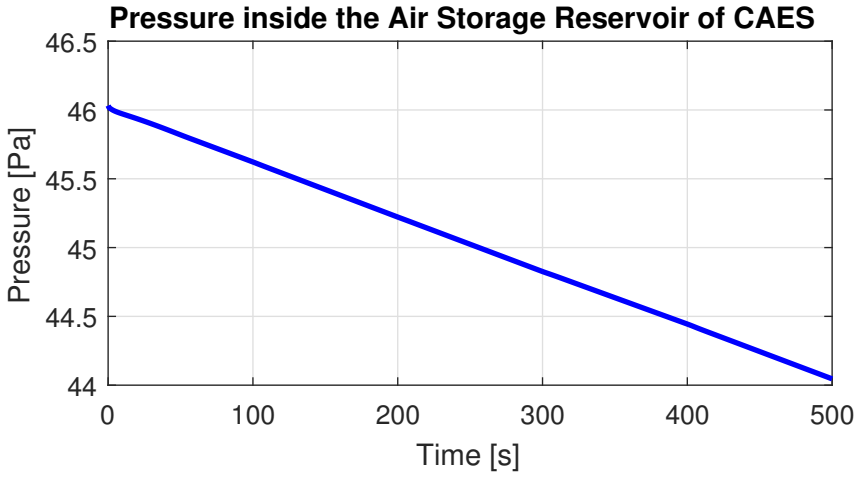

Fig. 4.15. Pressure of the air within the air storage reservoir

Figure 4.16 represents the torque that is provided by the CAES turbine. Turbine is coupled to the main motor/generator through torque coupling. In this method, the torques of the turbine and the main motor is added together and the output shaft is connected to the main generator. The torque coupling diagram is also shown in figure 4.17 [21]. In this type of coupling, the relationship of the speed and torque is expressed as:

$$\tau_{out} = \tau_{in1} i_{g1} + \tau_{in2} i_{g2} \tag{4.4}$$

where τ_{out} is the output torque, τ_{in1} is the first input torque, τ_{in2} is the second input torque, $i_{g1} = Z_2/Z_1$ is the gear ratio between the first and the second gear, $i_{g2} = Z_4/Z_3$ is the gear ratio between the third and fourth gear, and Z_1, Z_2, Z_3, Z_4 are the tooth number of the gears. The rotational speed of the output shafts can be expressed as:

$$\omega_{out} = \frac{1}{i_{g1}} \omega_{in1} \quad , \quad \omega_{in2} = \frac{i_{g2}}{i_{g1}} \omega_{in1} \tag{4.5}$$

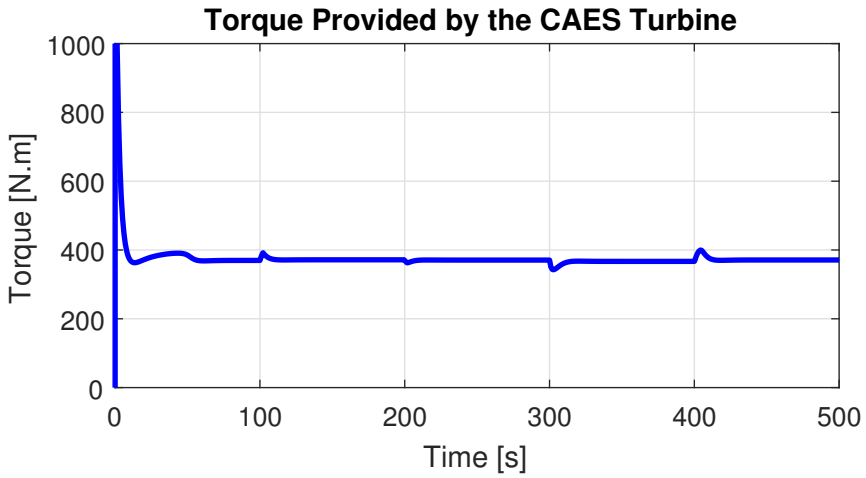

Fig. 4.16. Torque provided by the turbine of the CAES to the main generator

The coupling method can also be chosen as speed coupling method, in which the speed of the two input shafts are added together. Typical mechanism of this type of coupling is planetary gear unit, which is shown in figure 4.18. The planetary gear unit, also known as epicyclic gear train, consists of two gears mounted so that the center of one gear revolves around the center of the other. A carrier connects the

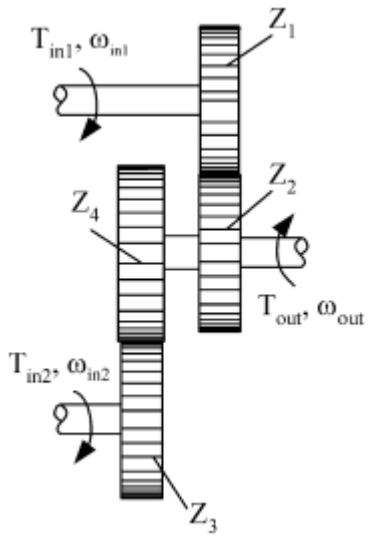

Fig. 4.17. Schematic of the torque coupling method

centers of the two gears and rotates to carry one gear, called the planet gear, around the other, called the sun gear. The relationship between the torque and the speed of the gears can be expressed as:

$$\omega_c = \frac{\omega_s}{1 + i_{sr}} + \frac{i_{sr}\omega_r}{1 + i_{sr}} \tag{4.6}$$

where ω_c is the angular velocity of the carrier, ω_s is the angular velocity of the sun gear, ω_r is the angular velocity of the ring, and $i_{sr} = Z_r/Z_s$ is the ratio of the tooth number of the ring to sun gear. The torque relationship can be expressed as:

$$\tau_r = i_{sr}\tau_s \qquad , \qquad \tau_c = (1 + i_{sr})\tau_s \tag{4.7}$$

where τ_r is the torque at the ring gear, and τ_s is the torque at the sun gear, $i_{sr} = Z_r/Z_s = R_r/R_s$, and R_r and R_s are the radius of the ring and sun gear, as can be seen in figure 4.18.

4.2 Maximum Power Point Tracking (MPPT)

The term power coefficient (C_p) generally describes the efficiency of the wind turbine and describes the ratio of the wind power absorbed to the available wind

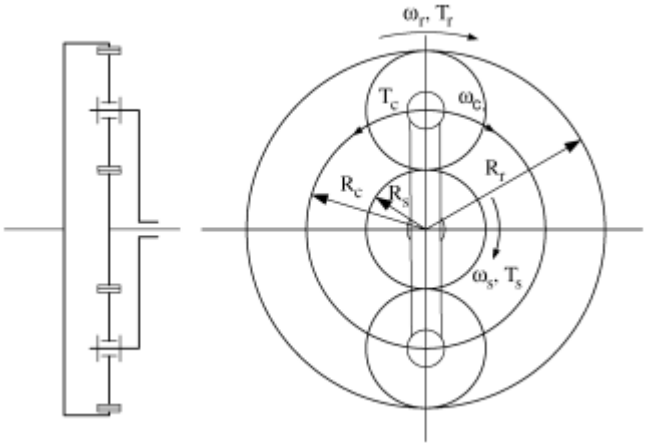

Fig. 4.18. Schematic of the speed coupling method

power. The mathematical description for this value is derived empirically by the turbine manufacturers; however, it generally follows a similar pattern and shape. The equation used in this paper is described in equation (2.2) and is depicted in Figure 2.2. As can be seen in the graph, the maximum power coefficient happens at a unique tip-speed ratio. The only variable in the tip-speed ratio, as described in the equation (2.4), that can be controlled is the rotational velocity of the turbine rotor so that the optimal tip-speed ratio can be achieved.

The most predominant factor in the operation of this system, as can be observed in the state-space equation (2.17), is the pressure variation. By changing the pressure of the system we can have control over the rotor speed. To do so, the method of varying the system pressure by altering the main motor load (τ_{L1}) and consequently optimizing the power coefficient is thereby proposed. Not only this method will result in increased efficiency and increased harvest of the wind power, it will also save money and cost by utilizing one of the integrated variables and eliminating the need for adding additional instruments to control the pressure.

If the objective is to optimize the power coefficient of a hydraulic wind power transfer system that only consists of one turbine, it is a single input - single output (SISO) system, in which the control input is the main generator load and the output

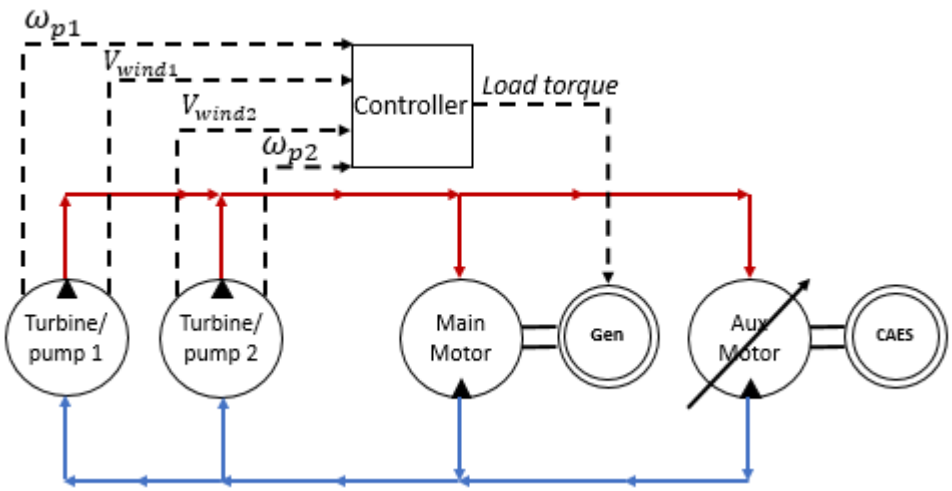

Fig. 4.19. Diagram of the control system for the Maximum Power Point Tracking (MPPT)

is the tip speed ratio λ corresponding to the highest point of C_p. This system can be easily controlled using an appropriate control strategy such as a PID controller. However, if our system consists of multiple wind turbines, in which each turbine occurs different wind speeds, our system becomes single input - multiple output (SIMO) system. In other words, we would like to optimize the power coefficient C_p of all the wind turbines using only main generator load. In this case, we would not be able to achieve the 100% of the power coefficient in every wind turbine but we would be able to increase the collective power obtained from all the wind turbines.

To control the amount of the load torque on the main generator, a suitable control strategy is necessary. The input to this controller is the rotational speed of the wind turbines and the effective wind speeds of each wind turbine. However, since 100% of the C_p is not achievable unless the wind speed of the both turbines are same, this controller takes the average of wind speeds and the average of rotational speed of the wind turbines as the input of wind speed to the controller.

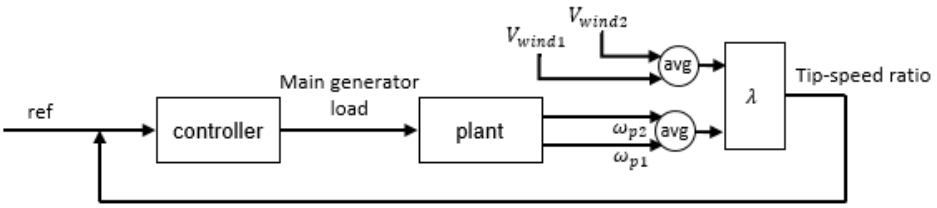

Fig. 4.20. Diagram of the control loop for the Maximum Power Point Tracking (MPPT)

The PID parameters are tuned manually by trial and error and familiarity to the system dynamic, and the resulting control law to control the load torque of the main generator is obtained as:

$$\tau_{L1} = 4000\left(\lambda_{ref} - \lambda(t)\right) + 100\int_0^{t_f}\left(\lambda_{ref} - \lambda(t)\right)dt \tag{4.8}$$

where τ_{L1} is the load torque on the main generator, λ_{ref} is the reference tip-speed ratio, and $\lambda(t)$ is the current tip-speed ratio. To obtain the $\lambda(t)$, the equation (1.3) is used and for the wind speed and turbine speed inputs, the average wind speed and turbine speed of all interconnected turbines is used. To test the described controller, a simulation has been conducted, and the wind speed profile of the figure 4.21 has been considered to be affecting a two interconnected hydraulic wind turbine. For the

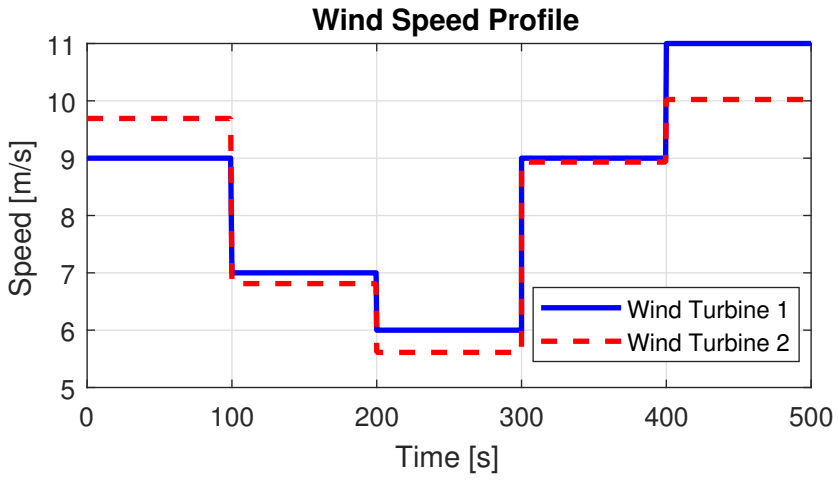

Fig. 4.21. Wind speed profile affecting the wind turbines

wind speed of the turbine 2, a random values with mean of 0, variance of 0.5, and sampling time of 100 seconds has been added to the speed of the first wind turbine to account for any possible disturbance and turbulences caused by the wind farm layout.

Figure 4.22 demonstrates the power coefficient (C_P) of the both wind turbines. As can be observed, the reason that the value of the power coefficient between the wind turbines differ is due to their difference in wind speed. This graph represents the power coefficient as a normalized value, meaning $C_P/C_{P(max)}$. The maximum power coefficient is considered to be 0.48, and the corresponding graph of the power coefficient versus the tip-speed ratio is shown in figure 2.2. As can be seen in figure 2.2, the maximum power coefficient occurs at a particular tip-speed ratio, regardless of the wind speed, and the objective of the controller is to keep the wind turbine rotor close to this value.

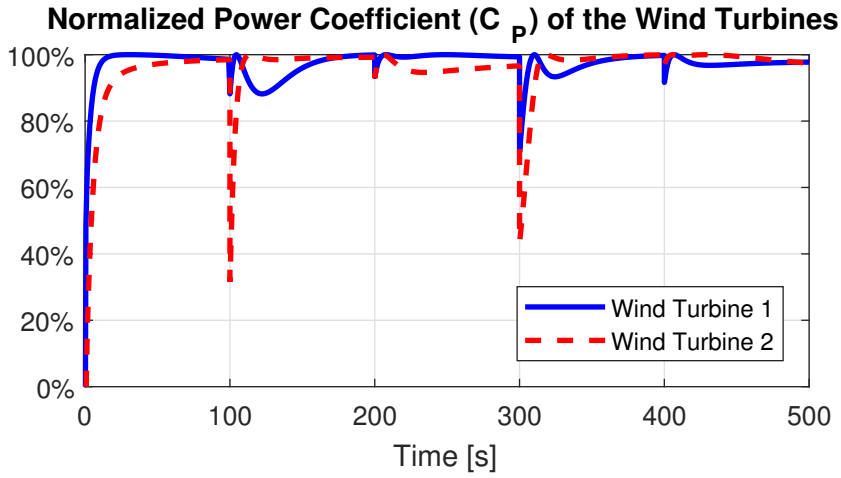

Fig. 4.22. The variations in the Power coefficient (C_P) as a result of the control strategy

Figure 4.23 demonstrates the control action, which is the load torque on the main generator. The torque exerted on the main generator changes the hydraulic pressure of the system, and since the pressure is the predominant factor in the hydraulic system, it affects the operation of the other interconnected components.

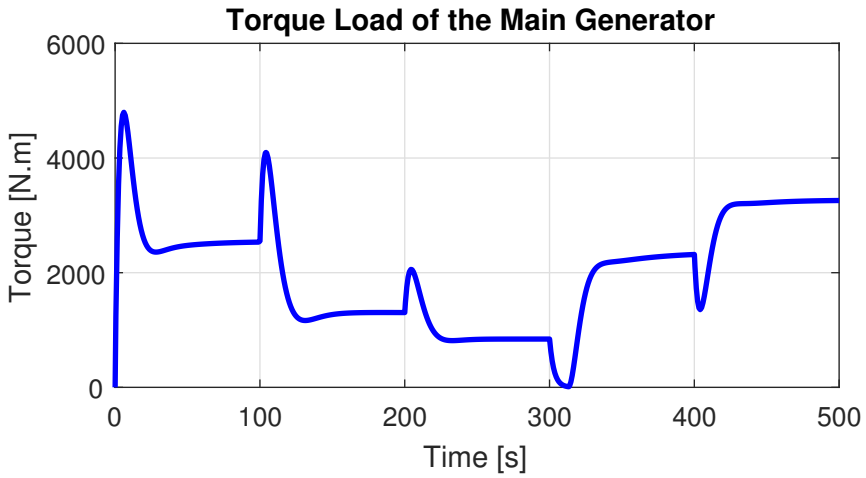

Fig. 4.23. Torque load on the shaft of the main generator

Figure 4.24 demonstrates the rotational velocity of the wind turbines' shafts. As can be noticed, the changes in the main generator load torque has caused variation in the wind turbine's speed, and has brought it closer to the maximum power point.

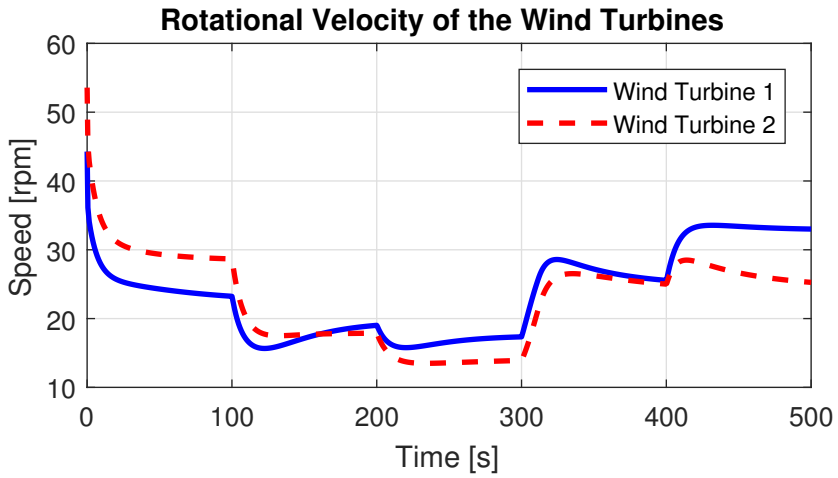

Fig. 4.24. Angular speed of the wind turbine shafts

Figure 4.25 depicts the hydraulic pressure of the system, which is the medium between the control action and the controller objective. The pressure is represented in the unit of Pascals, and the variation in the pressure is caused by the controller action.

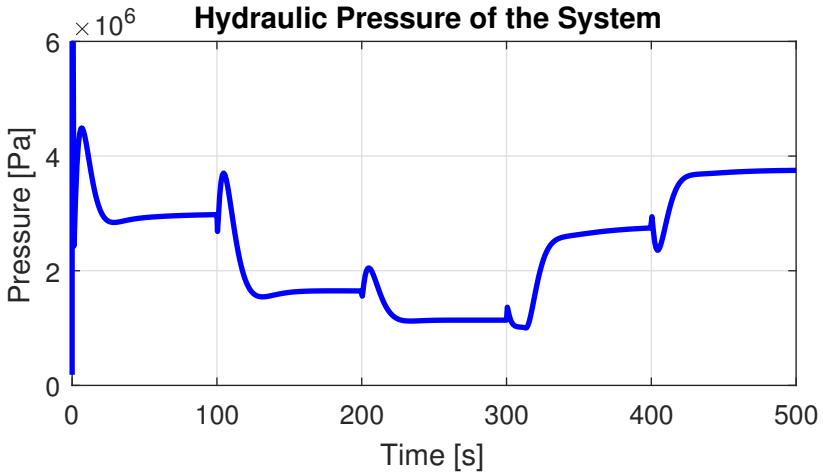

Fig. 4.25. Pressure of the hydraulic fluid within the system

5. RESULTS AND DISCUSSION

To validate the presented system dynamics and the control and optimization algorithms, a simulation environment needs to be created. The simulation was created in MATLAB/Simulink environment. Previously, to validate the dynamical equations, a test bench was designed, as shown in the Figure 2.1, and the dynamical equations were validated by comparing the simulations results with the test bench results [op&mod]. In this chapter, the system is simulated in various scenarios with all of the embedded control and optimization algorithms, that were discussed in the Chapter 4, in operation. The results provide a comprehensive understanding of the hydraulic system and its control algorithms and provides further insight into the operation of the hydraulic system and its control strategies.

5.1 High-Wind Simulation

During sufficient wind power condition, hydraulic flow rotates the main motor/generator at the required frequency, and the rest of the flow is directed to the auxiliary motor. This is done through the control system designed for the displacement of the auxiliary motor, as explained in the section 4.1.1. During this time, the CAES charges since the excess power is directed to the compressor by the auxiliary motor. As a result a pressure and temperature increase in the air storage reservoir is expected.

To simulate the high-wind condition, the wind speed profile of Figure 5.2 is considered to be impacting a two interconnected turbine system of the Figure 5.1. During the following simulation, all of the control systems explained in the Chapter 4 are turned active at $t_0 = 0$, and previous to that the wind speed of $10m/s$ and $12m/s$ were impacting the turbines 1 and 2, respectively, for a long time (steady-state). As can be

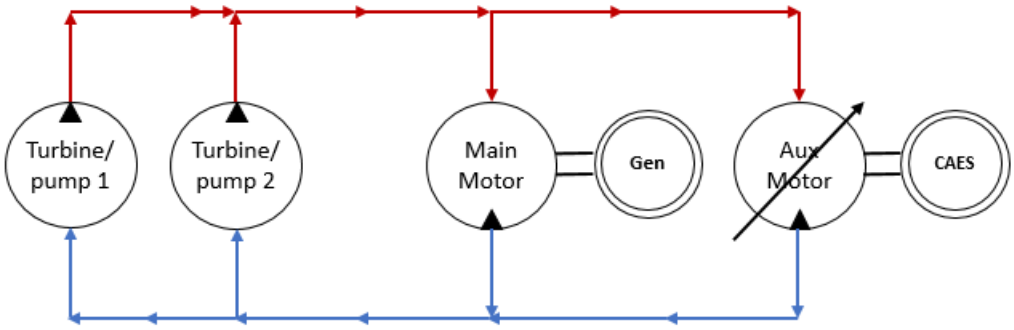

Fig. 5.1. Diagram of the Hydraulic Wind Power Transfer System (HWPTS) configuration used for the simulation

noticed in Figure 5.2, a slightly different wind speeds are considered to be impacting the both turbines to make sure this would not affect the operation of the integrated control systems. Different wind speeds can occur by the turbulences caused by the environmental obstructions and the general wind farm layout. This difference and turbulences reduce in higher altitudes, which is desirable especially for more powerful wind turbines.

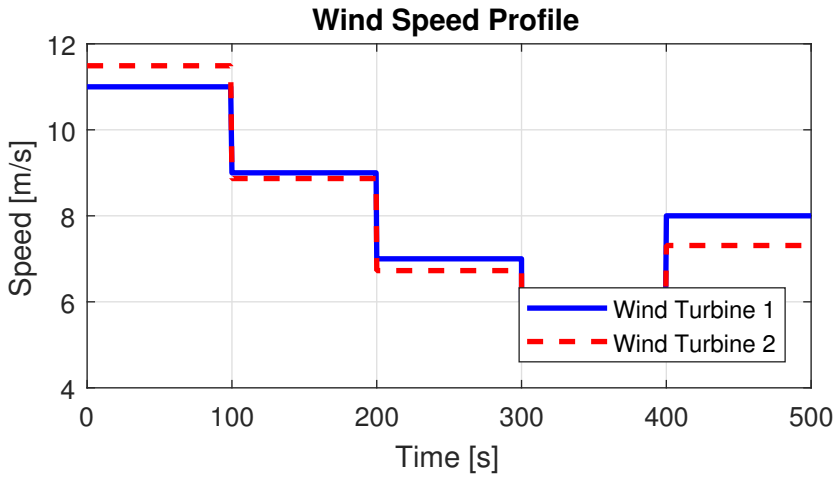

Fig. 5.2. Wind speed profile affecting the two turbines

Figure 5.3 demonstrates the rotational speed of the turbine blades when the control systems become active at $t_0 = 0$. The speed variation of the turbines are mainly

caused by the maximum Power Coefficient (C_P) control, as explained in the section 4, which is also referred to as Maximum Power Point Tracking (MPPT). Comparing the graph of Figure 5.3 with Figure 5.5 gives a better insight on the effect of the turbine speed change on the Power Coefficient of the turbine.

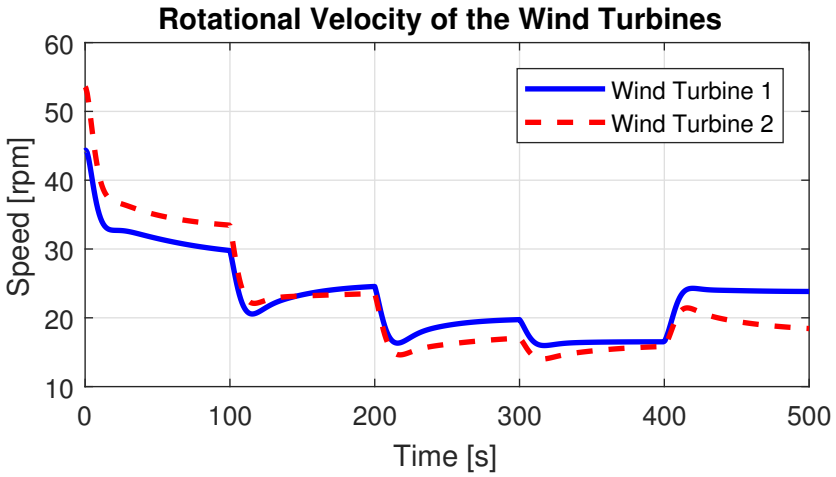

Fig. 5.3. Angular speed of the wind turbine shafts

Figure 5.4 demonstrates the graph of the main generator frequency. As can be observed, frequency variation of the main generator is minimized as a result of the control strategy explained in section 4.1.1, and the maximum frequency variation is 0.05% during the simulation.

Figure 5.5 is the graph of the normalized Power Coefficient (C_P) of the both turbines. C_P is similar to efficiency and the higher values show a higher absorption rate of power from the available wind power. It affects the wind power absorption according to the equation 2.1. The maximum C_P value for both turbines are considered to be 0.48, and based on that, a normalized graph is presented in Figure 5.5.

Changes in the C_P value impacts the amount of the power absorbed by the wind turbine blades. Even though the rotational speed of the turbine blades rises above the optimum C_P point, the exerted torque, and as a result the obtained power from the wind reduces, and thus the optimum C_P controller follows the maximum power

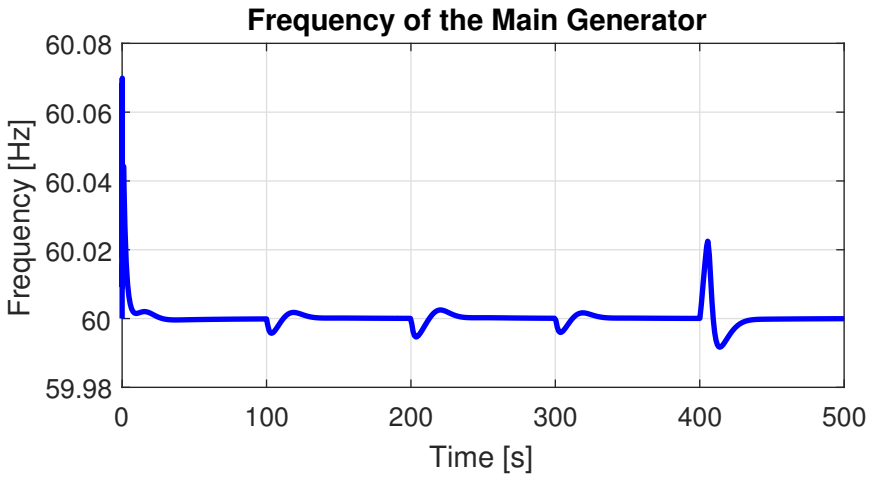

Fig. 5.4. Frequency of the main generator shaft

point. Figure 5.6 demonstrates the power obtained from the wind turbine blades during the time of the simulation.

Auxiliary motor is placed in the system to absorb the excess hydraulic fluid of the system, and store its energy in Compressed Air Energy Storage (CAES). Auxiliary motor's displacement is controlled to obtain a constant frequency for the main

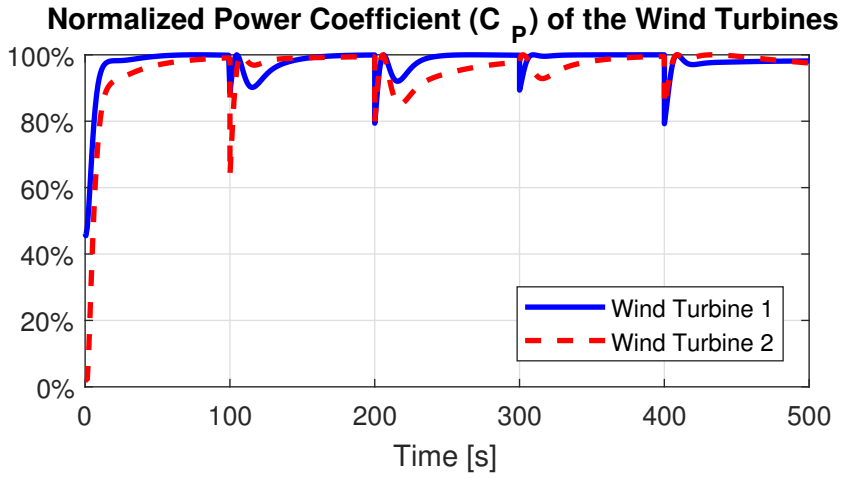

Fig. 5.5. The variations in the Power coefficient (C_P) as a result of the control strategy

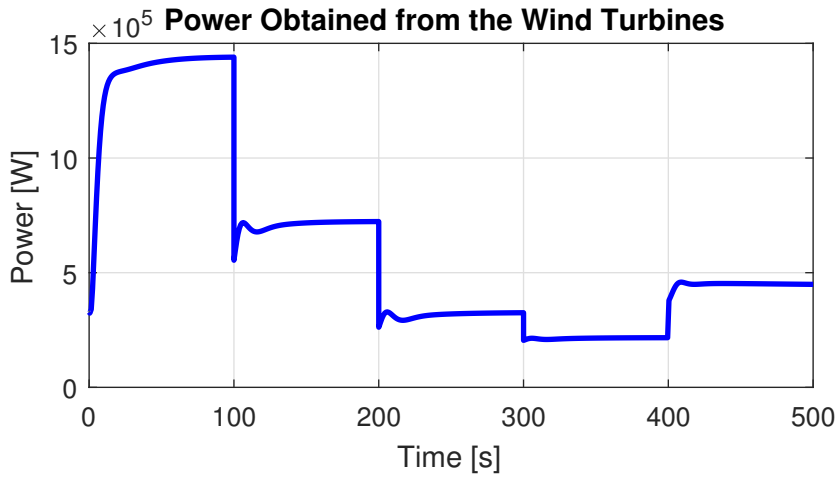

Fig. 5.6. The total wind power absorbed from the wind by the wind turbines

motor/generator during wind fluctuations, as explained in the section 4.1.1. Figure 5.7 demonstrates the rotational velocity of the auxiliary motor, which is connected to the compressor stage of the CAES.

Figure 5.8 demonstrates the variation in the auxiliary motor displacement that is utilized to control the frequency of the main generator.

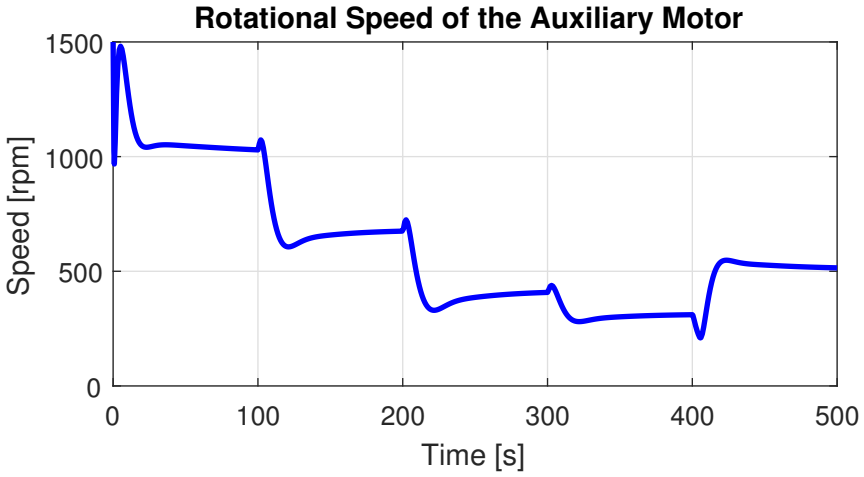

Fig. 5.7. Angular velocity of the shaft of the auxiliary motor

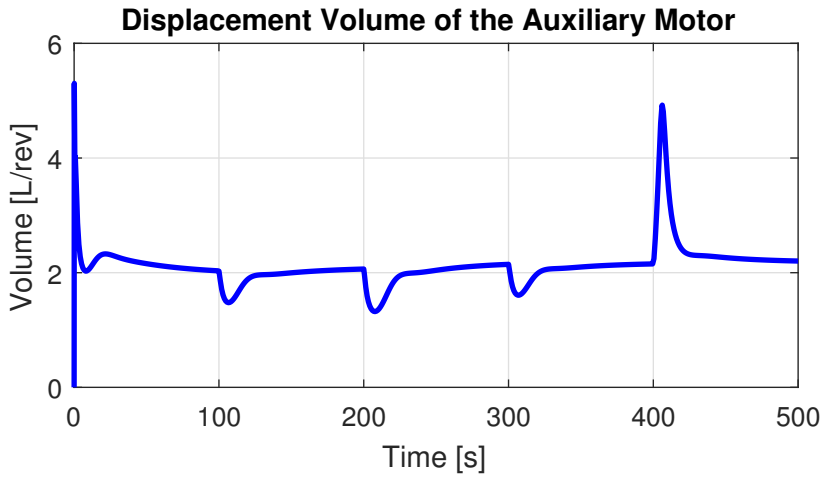

Fig. 5.8. Displacement variations of the variable-displacement auxiliary motor

Figure 5.9 demonstrates the hydraulic pressure inside the system pipes. As can be noticed in the system's state-space representation, which was described in equation 2.17, pressure variation affects the operation of every component in the system. Every control system that was also designed for this system, takes advantage of the significance of hydraulic pressure. System's maximum pressure depends on the specifications of the hydraulic motors and pumps and the pressure tolerance of the pipes,

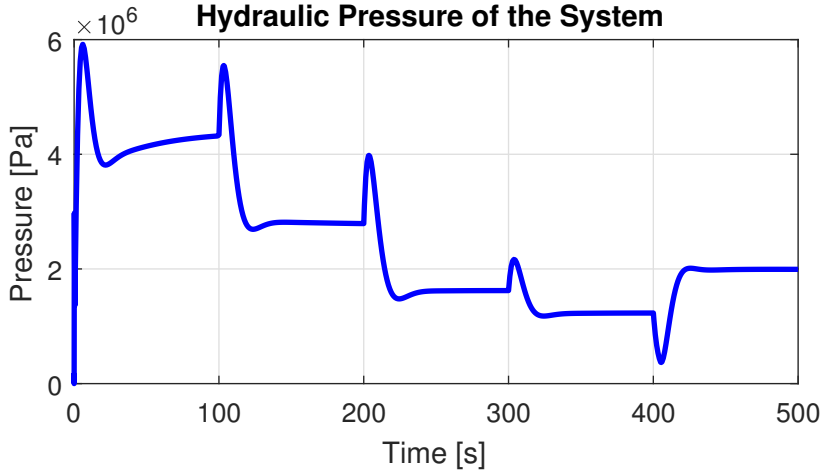

Fig. 5.9. Pressure of the hydraulic fluid within the system

and based on that appropriate pressure relieve valves can be installed in the system to prevent damages to the system components.

Figure 5.10 demonstrates the pressure inside the air storage reservoir during the simulation period. As can observed, the storage pressure increases when there is sufficient wind which indicates the charging mode.

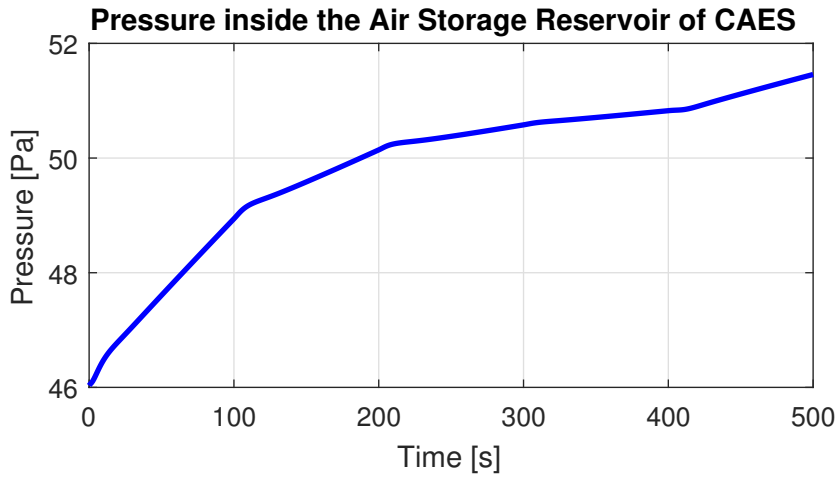

Fig. 5.10. Pressure of the air within the air storage reservoir of the CAES

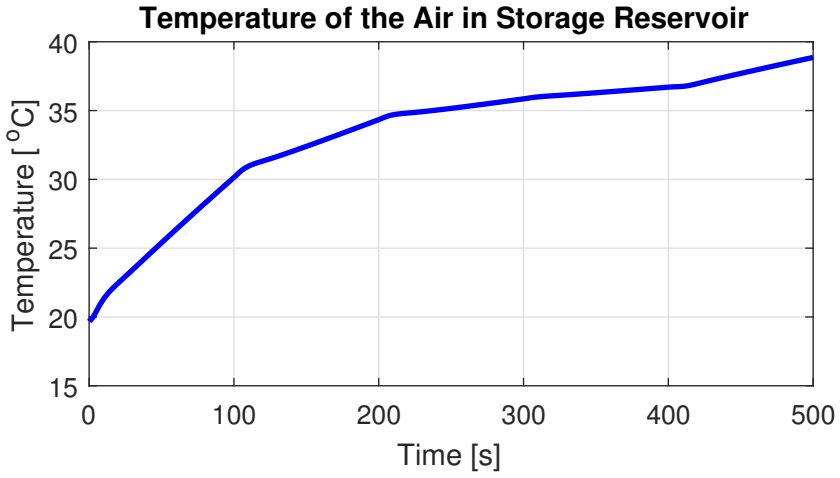

Fig. 5.11. Temperature of the air within the air storage reservoir of the CAES

Considering the air to be an ideal gas, the temperature of the air inside the air storage reservoir can be obtained using the ideal gas law as explained in equation 3.3. This temperature is shown in the Figure 5.11. For the calculation of temperature, air storage cavern is considered to be insulated. However, certain imperfections in the sealing and reservoir structure can slightly affect the temperature.

5.2 Low-Wind Simulation

During some periods, wind speed might not be enough to keep the main generator in constant frequency. To resolve this issue, an energy storage technology can be integrated so that the extra energy from the high-wind periods can be restored to the system and balance the energy production. A Compressed Air Energy Storage (CAES) is considered as the primary energy storage device for this purpose.

As was discussed in the section 4.1.2, a proper controller is needed to provide the required torque from the CAES to the main motor/generator shaft in order to produce a constant frequency power. In order to regulate the CAES torque, two possible scenarios can be considered which are either controlling the mass flow rate of the air coming out of the air storage reservoir, or the geometry of a possible variable-geometry turbine. For the purpose of simulation, we have considered a fixed geometry turbine, and have designed a controller for the mass flow rate of the air, as explained in section 4.1.2.

In this section, we have simulated the system of two interconnected wind turbines and have presented the results. Figure 5.12 shows the wind speed profile that is affecting both wind turbines. As can be noticed, the wind speeds affecting the wind turbines are slightly different to account for the possible disturbances by the environmental obstacles.

Based on the available wind power and the feedback from the main generator frequency, the controller alters the mass flow rate of air exiting the air storage reservoir and determines the torque that is needed from the CAES. The high pressure air causes

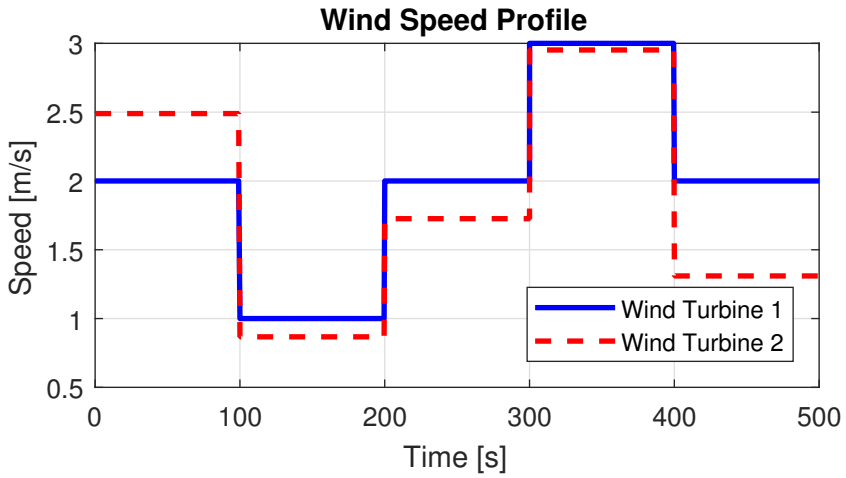

Fig. 5.12. Wind speed profile affecting both turbines

the turbine to rotate and provide the required torque to the main generator shaft. Figure 5.13 shows the torque that is exerted by the turbine shaft on the main generator shaft.

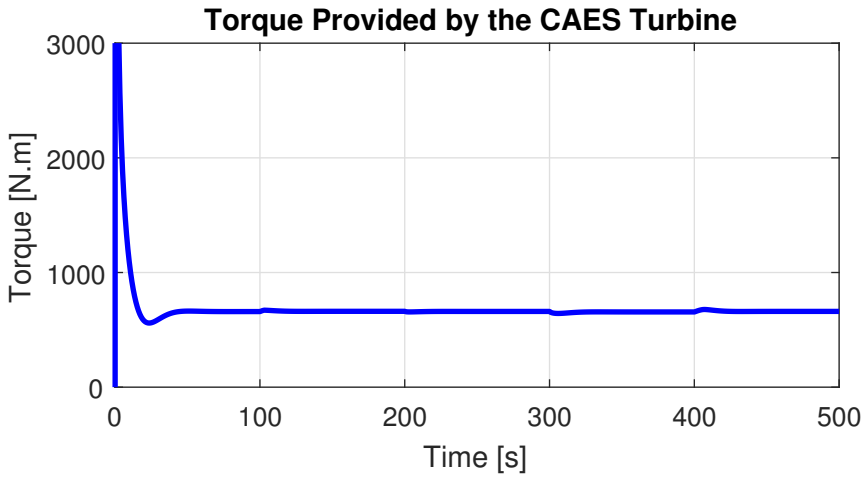

Fig. 5.13. Torque provided by the turbine of the CAES to the main generator

The objective of the controller is to keep the main generator at a constant frequency. The resulting main generator frequency from the controller action is shown in the figure 5.14. In the beginning of the simulation, the wind turbines and the main

generator were at rest, and thus, the frequency starts from 0 Hz and reaches the 60 Hz.

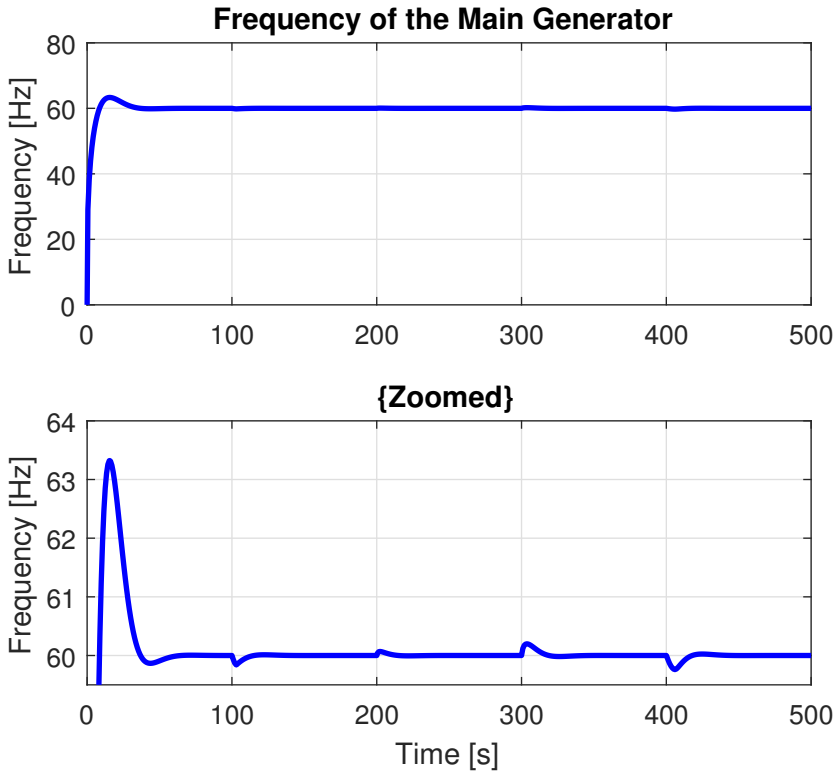

Fig. 5.14. Frequency variation of the main generator

Figure 5.15 demonstrates the control action of the CAES, which is the mass flow rate of the air impacting the turbine. The turbine provides the remaining torque for the main generator. The mass flow rate of the air can be controlled using a proportional valve, or alternatively a constant mass flow rate of air can be coupled using an On/Off valve to a variable geometry turbine. In this simulation a proportional valve is considered to be altering the air mass flow rate.

Figure 5.16 demonstrates the pressure of the air inside the air storage reservoir. As can be noticed, the pressure drops as it provides the stored energy back to the system. Air pressure loss through the valve sealings have not been accounted for and can be minimized through proper sealing.

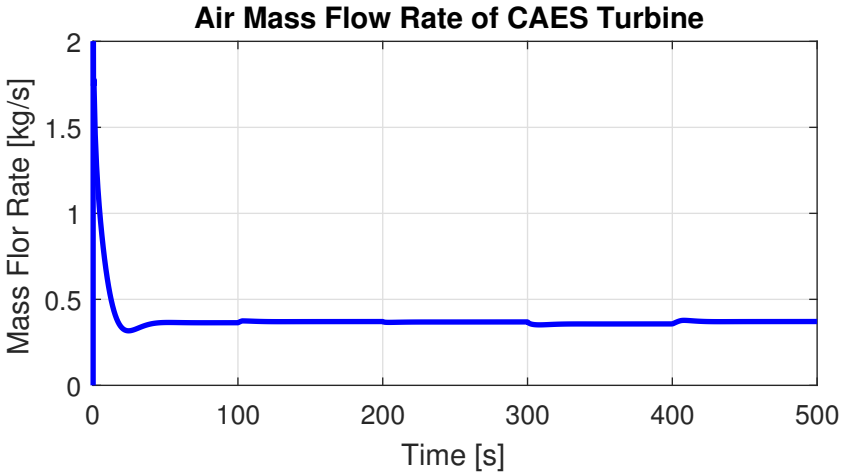

Fig. 5.15. Frequency variation of the main generator

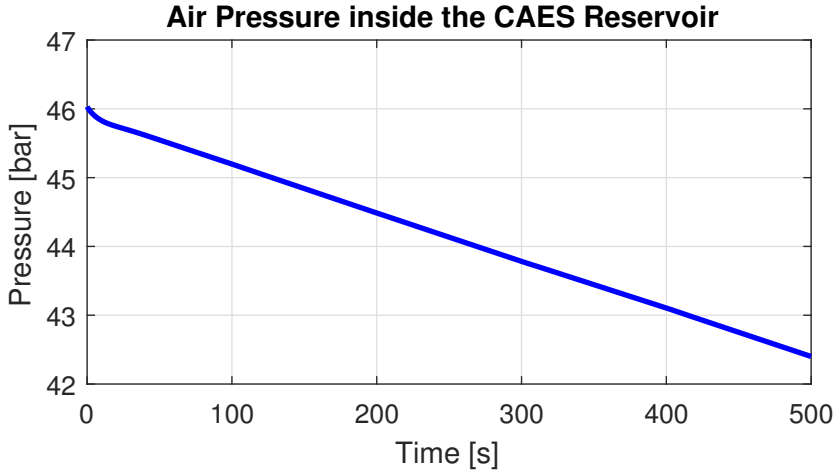

Fig. 5.16. Pressure of the air inside the air storage reservoir of the CAES

Figure 5.17 demonstrates the temperature of the air inside the air storage reservoir. The air inside is considered to be ideal gas and thus the equation of 3.3 would be applicable here. The temperature loss through the air storage walls are negligible and can be minimized through proper insulation.

Figure 5.18 demonstrates the power that has been provided by the compressed air to keep the main generator at a steady frequency. The part of the power is provided by the wind turbines and the rest of the required power is provided by the CAES.

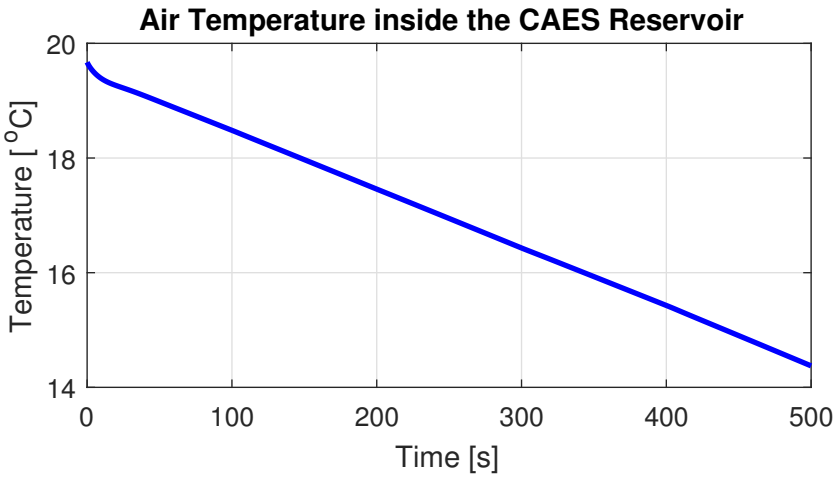

Fig. 5.17. Temperature of the air inside the air storage reservoir of the CAES

In this simulation, since the wind turbine was stationary at $t = 0s$, the compressed air is utilized to run the main generator from the stationary position. Since the wind speed profile includes the cut-off wind speeds, the main generator is mainly run with the power of the CAES.

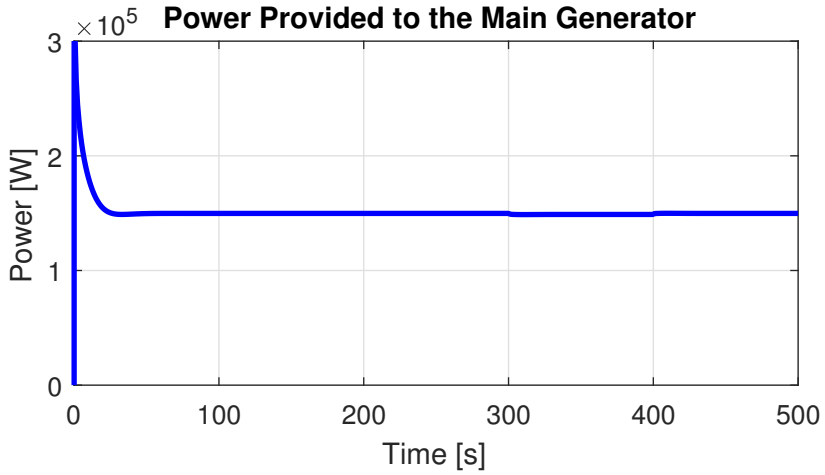

Fig. 5.18. Power delivered to the main generator

The rotational speed of the CAES turbine is shown in figure 5.19 which is used to keep the frequency of the main generator steady. The turbine is coupled to the

main generator shaft through torque coupling, which was discussed in the previous chapter.

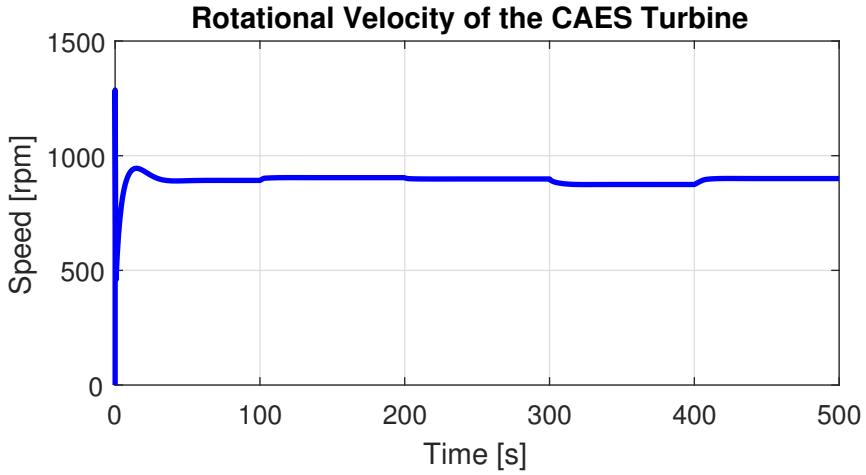

Fig. 5.19. Angular Speed of the CAES turbine

5.3 Combined High and Low Wind

In this section, we have examined a wind speed profile that consists of a speed from high to lower wind. This simulation would ensure the proper working of the controllers described in the previous chapter. For this purpose the wind speed profile of the figure 5.20 is used for the simulation which includes a variety of wind speeds.

Figure 5.21 demonstrates the angular speed of the wind turbine shaft. As can be noticed, during the low-wind and cut-off wind speeds, the wind turbine velocity declines to near zero, and is not able to keep the main generator at a constant frequency.

Figure 5.22 demonstrates the power obtained from wind, obtained by the main generator, obtained by the auxiliary generator, and provided by the CAES. As can be noticed, as soon as the wind is not able to provide the power required for the rotation of the main generator, the CAES begins to provide the remaining power.

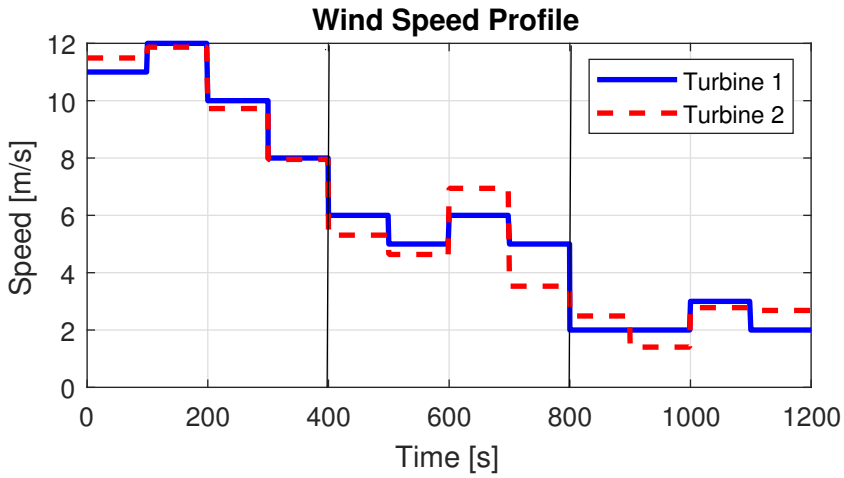

Fig. 5.20. Wind speed profile affecting the both turbines

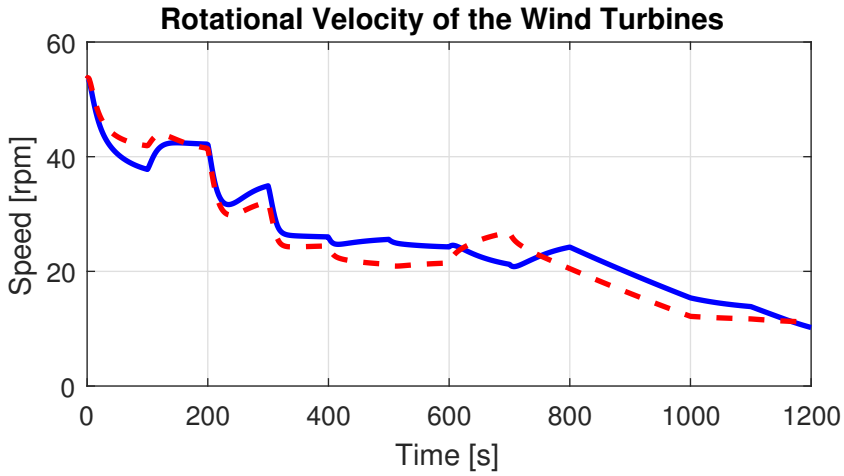

Fig. 5.21. Angular speed of the both turbines

Figure 5.23 shows the frequency of the main generator. As can be noticed, the frequency variation is minimized using the appropriate control algorithms during high and low wind conditions. Switching algorithm between these algorithms is also critical to ensure the stability of the system. To do so, a switching algorithm is designed to switch to CAES control when the displacement of the auxiliary motor reaches 0, and to switch to auxiliary motor displacement control when the displacement is above 0.

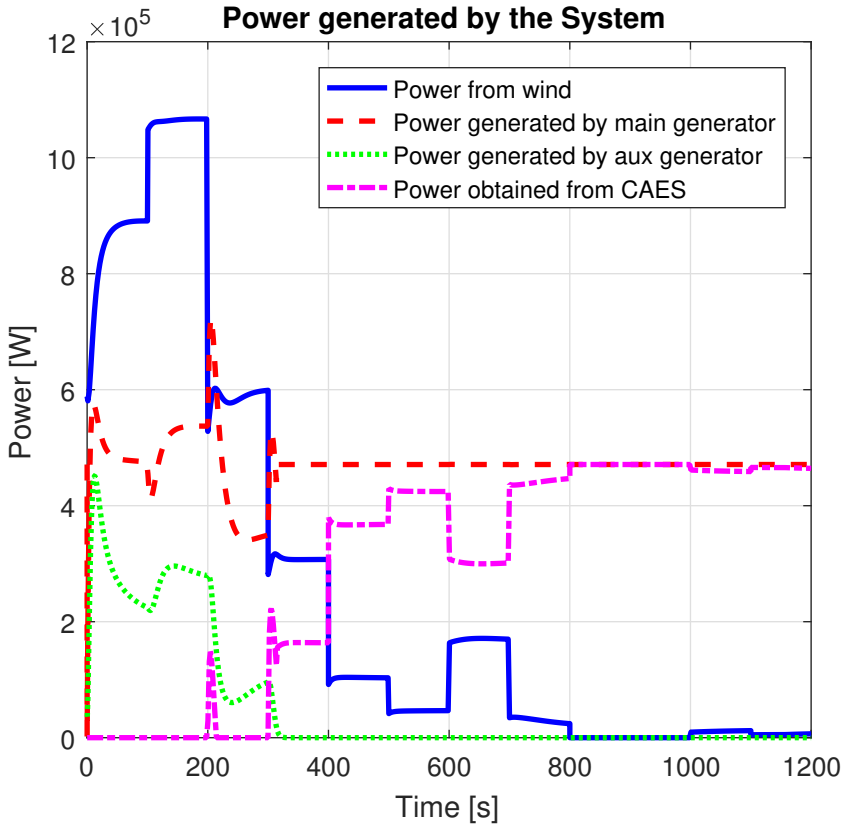

Fig. 5.22. Total power absorbed by the wind turbines from the wind

This would ensure that correct operation of the system without dependability to the external or state values, since they are prone to change.

Figure 5.24 demonstrates the load torque exerted on the main generator, which is the control action of maximizing the power coefficient. When there is enough wind speed, the load torque is varied to ensure the power coefficient (C_P) is maximized. However, when the wind is low and the power is being provided by the CAES, the torque is changed proportionally to the electrical demand.

The pressure profile of the hydraulic flow within the system is shown in figure 5.25. The hydraulic pressure is the predominant factor in the operation of hydraulic system, and is mathematically described in equation 2.17.

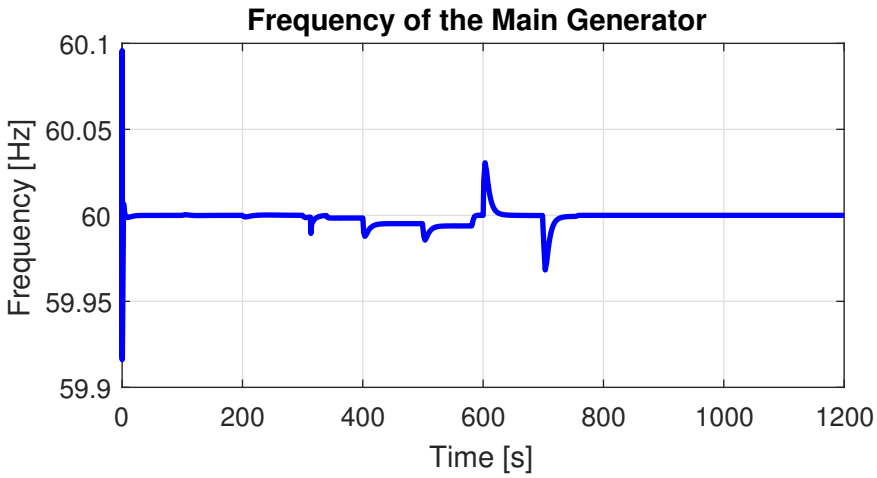

Fig. 5.23. Frequency of the main generator

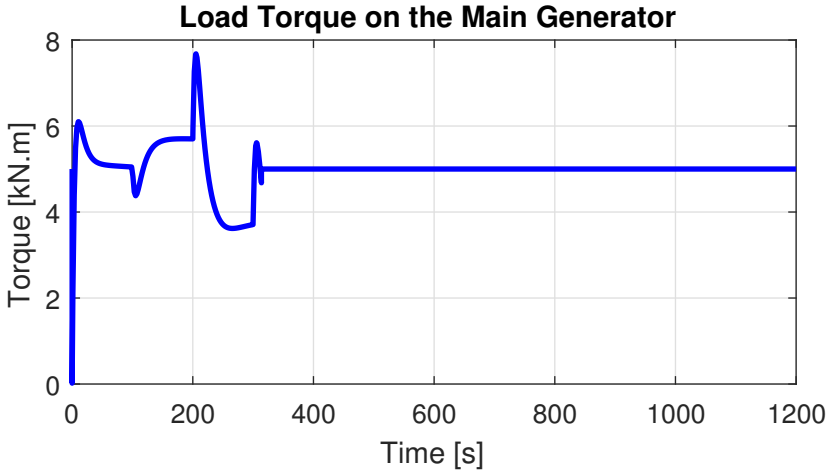

Fig. 5.24. Load torque exerted on the main generator

The turbine runs by directing the stored pressurized air toward the turbine. Therefore, the speed of the turbine can be controlled by controlling the air mass flow rate of the air that is exiting the air storage, which is shown in figure 5.26.

Figure 5.27 demonstrates the response of the displacement of the auxiliary motor. The controller action alters the displacement of the auxiliary motor in order to keep the main generator frequency constant.

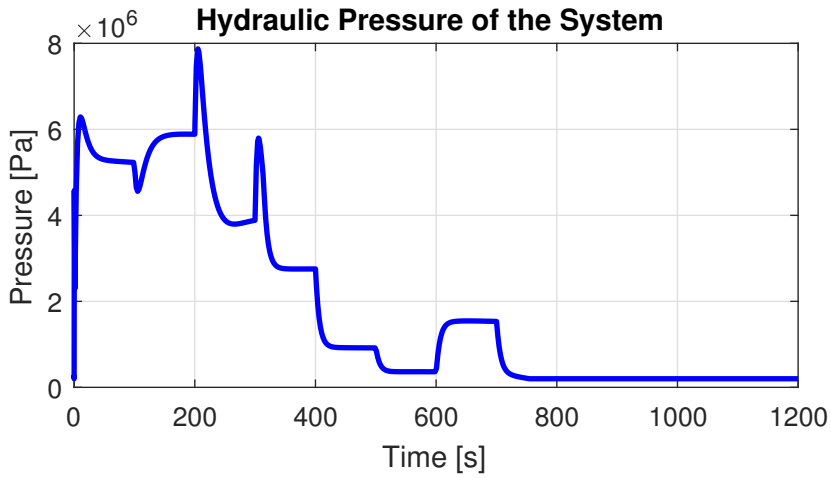

Fig. 5.25. Pressure of the hydraulic fluid within the system

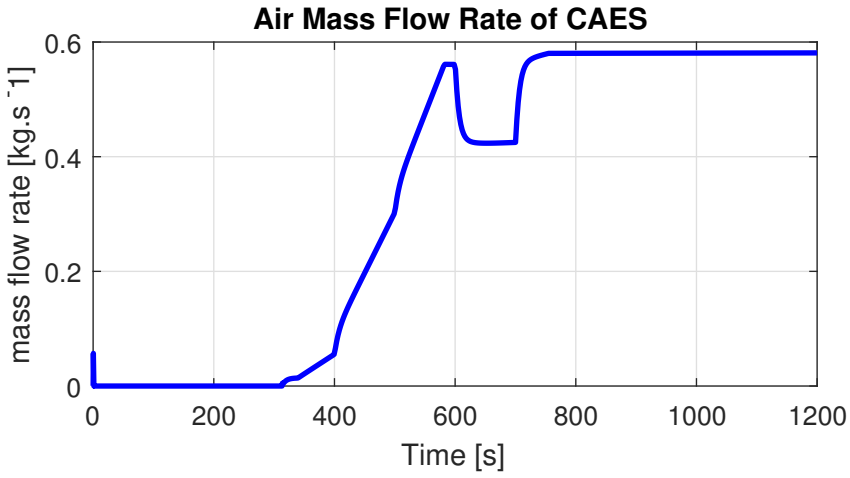

Fig. 5.26. Mass flow rate of the air exiting the CAES to run the turbine

The angular speed of the auxiliary motor is shown in figure 5.28. Changes in the speed is caused by the action of all the control inputs and disturbances involved. When there is not sufficient wind power, the speed of the auxiliary motor drops to zero.

Air pressure inside the air storage reservoir is shown in figure 5.29. As can be seen, the air storage pressure rises according to the excess energy that is available in

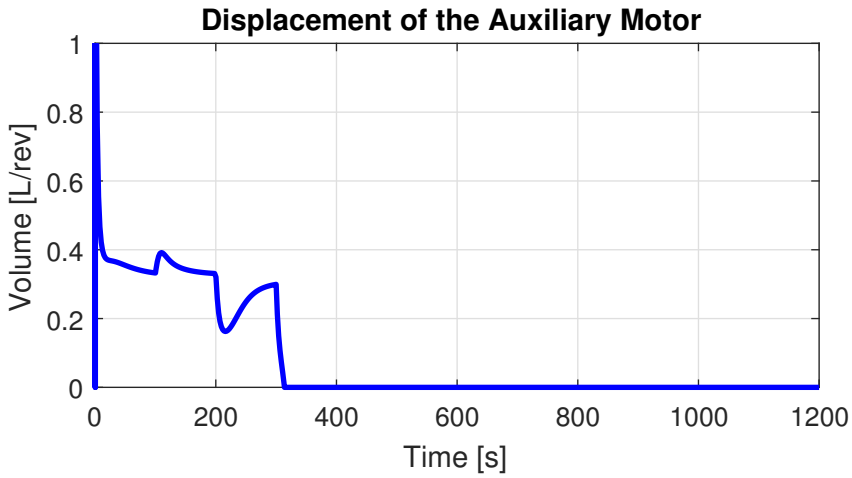

Fig. 5.27. Displacement variations of the variable-displacement auxiliary motor

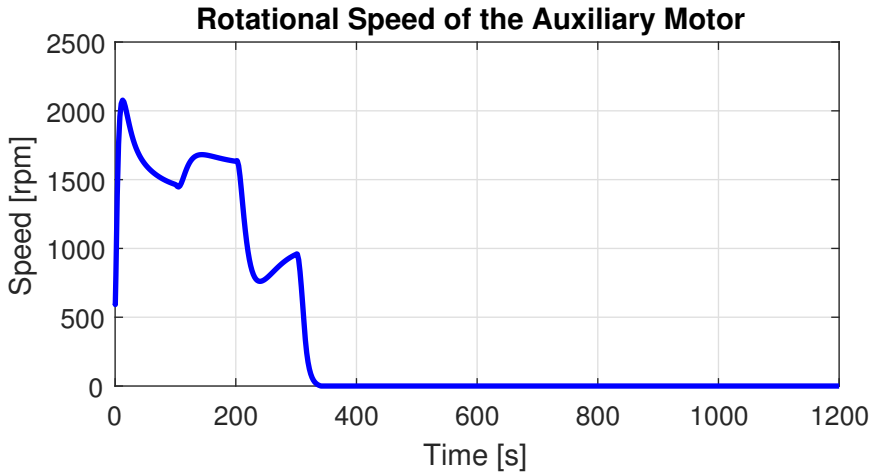

Fig. 5.28. Angular velocity of the auxiliary motor shaft

wind, and therefore, when the wind speed is not sufficient enough, the CAES starts providing power and the pressure starts dropping.

The temperature of the air inside the reservoir is shown in figure 5.30. The air is considered to be an ideal gas, and the temperature is proportional to its pressure.

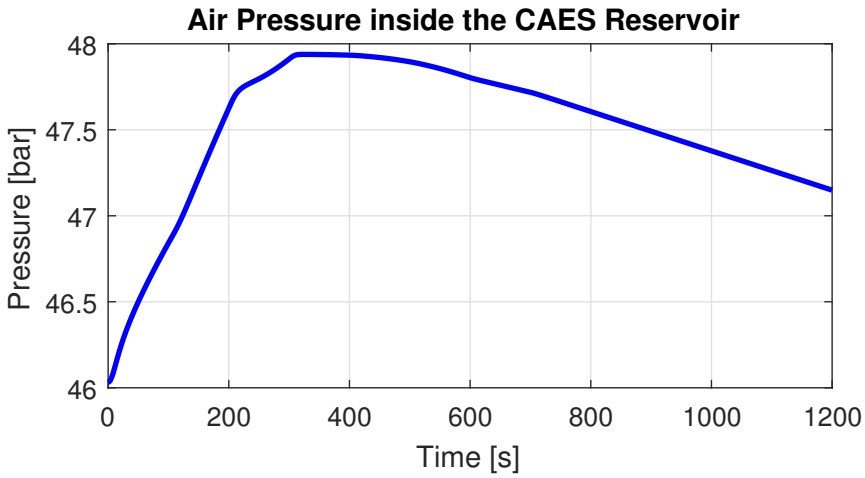

Fig. 5.29. Pressure of the air stored in the CAES reservoir

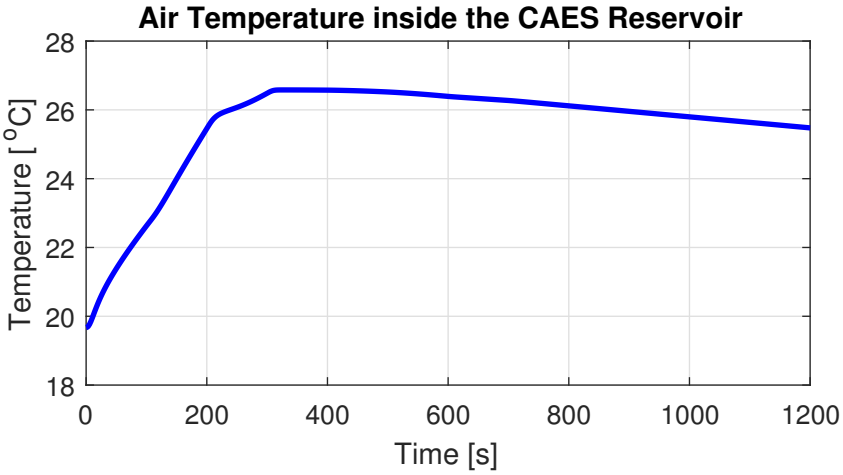

Fig. 5.30. Temperature of the air stored in the CAES reservoir

6. SUMMARY

This thesis has introduced and studied the governing equations of the hydraulic wind power transfer system. This system, which uses pressurized hydraulic fluid as the medium to transfer the wind energy, has significant economical advantages over the conventional wind turbine technology. The modeling and the response of the system with respect to different wind conditions are discussed, and the behavior of the system is shown using the graph of the state variables of the system.

Furthermore, due to the unreliability of renewable energies, a compressed air energy storage system has been introduced to couple with hydraulic wind power transfer system to store the excess energy during the periods when the wind power is more than the demand, and return it back to system when the wind power cannot meet the demand. The equations of this system has been introduced and the method of coupling has been discussed.

In addition, the control strategies of this system has been revised and shown. Two of the control strategies that have been introduced, aim to improve the power quality and match the grid regulations during the periods of high-wind and low-wind. Each of these periods require a separate controller to keep the frequency of the main generator steady. The third controller that was introduced, aims to increase the efficiency of the system and achieve the maximum power point. This controller ensures that the maximum available power is absorbed by the wind turbines.

Finally, the simulation results of the system are shown in the last chapter. These results shows the state variable, control actions, and system outputs during multiple scenarios. The results demonstrate the successful operation of hydraulic wind power transfer system, with its integrated controllers and energy storage system.

7. RECOMMENDATIONS

Hydraulic wind power transfer system has a very high potential to replace the conventional wind turbines. This technology is able to provide a significantly cost effective solution to harvest the wind energy, which can further expand the wind turbine capacity of the world even at a faster rate. This thesis has provided a mathematical and engineering insight into making this technology a reality. To further improve the prototype of this technology, I can recommend the following points:

- Wind speed estimation is an important part of the operation of the wind turbine and its control systems. Using wind speed data, we can achieve higher efficiencies and prevent the wind turbine damage from very high wind speeds. Currently, anemometers are installed in wind turbines to measure the wind speed. However, due to the turbulences that occur before and after the wind turbine blades, anemometers might not provide an accurate data on wind speed, and using an anemometer on every wind turbine might end up costly. I would recommend a method of wind speed estimation using system's state variable data. By finding a relation between the variables of the system and the wind speed, we can eliminate the need for anemometers, and simply estimate the wind speed using the system variables.

- To be able to provide an even more cost-effective configuration of hydraulic wind power transfer system, each component of the system should be optimally sized. This would ensure that the proposed system not only is able to meet the required demand, it also providing the most affordable solution. To do so, an objective function of the system cost needs to prepared, and the constraints of the system regarding the minimum and maximum electrical demand and maximum speed and torque tolerance of the pumps, motors and generator must be set.

REFERENCES

REFERENCES

[1] United Nations Commission of Sustainable Development, *Framing Sustainable Development The Brundtland Report – 20 Years On*, Backgrounder, April 1, 2007.

[2] REN21, *Renewables 2017 global status report*. (Paris: REN21 Secretariat). *On the electrodynamics of moving bodies*, ISBN 978-3-9818107-6-9, Pages 1-20, March 13, 2017.

[3] U.S. Department of Energy (DOE), *U.S. Energy and Employment Report*, January 5, 2017.

[4] MIT Wind Energy Group & Renewable Energy Projects in Action, *Wind Power Fundamentals*, January 10, 2010.

[5] DOE Office of Energy Efficiency and Renewable Energy, Retrieved from: https://www.energy.gov/eere/wind/inside-wind-turbine-0, Accessed on March 20, 2018

[6] Ayana Pusha, Afshin Izadian, Majid Deldar, *Energy Efficiency and Loss Analysis of Hydraulic Wind Power*, IEEE International Conference on Electro-Information Technology, Rapid City, SD, May 9-11, 2013.

[7] Compressed Air Energy Storage (CAES), Retrieved from: http://energystorage.org/compressed-air-energy-storage-caes, Accessed on February 15, 2018

[8] Xing Luo, Jihong Wang, Mark Dooner, Jonathan Clarke, *Overview of current development in electrical energy storage technologies and the application potential in power system operation*, Elsevier Applied Energy Volume 137, Pages 511-536, January 1, 2015.

[9] Haisheng Chen, Thang Ngoc Cong, Wei Yang, Chunqing Tan, Yongliang Li, Yulong Ding, *Progress in electrical energy storage system: A critical review*, Elsevier Progress in Natural Science Volume 19, Issue 3, Pages 291-312, March 10, 2009.

[10] Matthias Finkenrath et al., *Status and Technical Challenges of Advanced Compressed Air Energy Storage (CAES) Technology*, 2009 International Workshop on Environment and Alternative Energy Organized by C3P and NASA, GE Global Research, Garching n. Munich, Germany, November 10-13, 2009.

[11] Afshin Izadian, Sina Hamzehlouia, Majid Deldar, Sohel Anwar, *Hydraulic Wind Power Transfer System: Operation and Modeling*, IEEE Transactions on Sustainable Energy, Volume 5, Issue 2, Pages 457-465, January 10, 2014.

[12] Mohsen Farbood, Elaheh Taheran Fard, Mokhtar Sha-Sadeghi, Afshin Izadian, Taher Niknam, *Modeling and control of interconnected wind turbines drivetrains*, 2017 IEEE Energy Conversion Congress and Exposition (ECCE), November 7, 2017.

[13] A. Esposito, *Fluid Power with Application*, 7th ed., Englewood Cliffs, NJ, USA: Prentice-Hall, March 1, 2009.

[14] A. V. Akkaya, *Effect of bulk modulus on performance of a hydrostatic transmission control system*, Sadhana, Volume 31, Issue 5, Pages 543–556, October 1, 2006.

[15] Fernando De Samaniego Steta, *Modeling of an Advanced Adiabatic Compressed Air Energy Storage (AA-CAES) Unit and an Optimal Model-based Operation Strategy for its Integration into Power Markets*, Swiss Federal Institute of Technology (ETH) Zurich, October 5, 2010.

[16] M. M. El-Wakil, *Powerplant Technology*, Singapore, McGraw-Hill, Chapter 16, Section 2, Pages 680-685, March 5, 1998.

[17] Majid Deldar, Afshin Izadian, Masoud Vaezi, Sohel Anwar, *Modeling of a Hydraulic Wind Power Transfer Utilizing a Proportional Valve*, IEEE Transactions on Industry Applications, Volume 51, Issue 2, Pages 1837-1844, September 8, 2014.

[18] M. Osman Abdalla, T. Nagarajan, Mohed H. Fakhruldin, *Numerical study of flow field and energy loss in hydraulic proportional control valve*, 2011 National Postgraduate Conference, January 23, 2012.

[19] J. G. Ziegler and N. B. Nichols, *Optimum Settings for Automatic Controllers*, Journal of Dynamic Systems, Measurement, and Control, Volume 115, Issue 2B, Pages 220-222, June 1, 1993.

[20] Bjorn D. Tyreus, and William L. Luyben, *Tuning PI controllers for integrator/dead time processes*, Industrial and Engineering Chemistry Research, Volume 31, Issue 11, Pages 2625-2628, November 10, 1992.

[21] Gao Y., Ehsani M., *A torque and speed coupling hybrid drivetrain-architecture, control and simulation*, IEEE Transactions on Power Electronics, Volume 21, Issue 3, Pages 741-748, May 8, 2006.

APPENDICES

A. BLOCK DIAGRAM

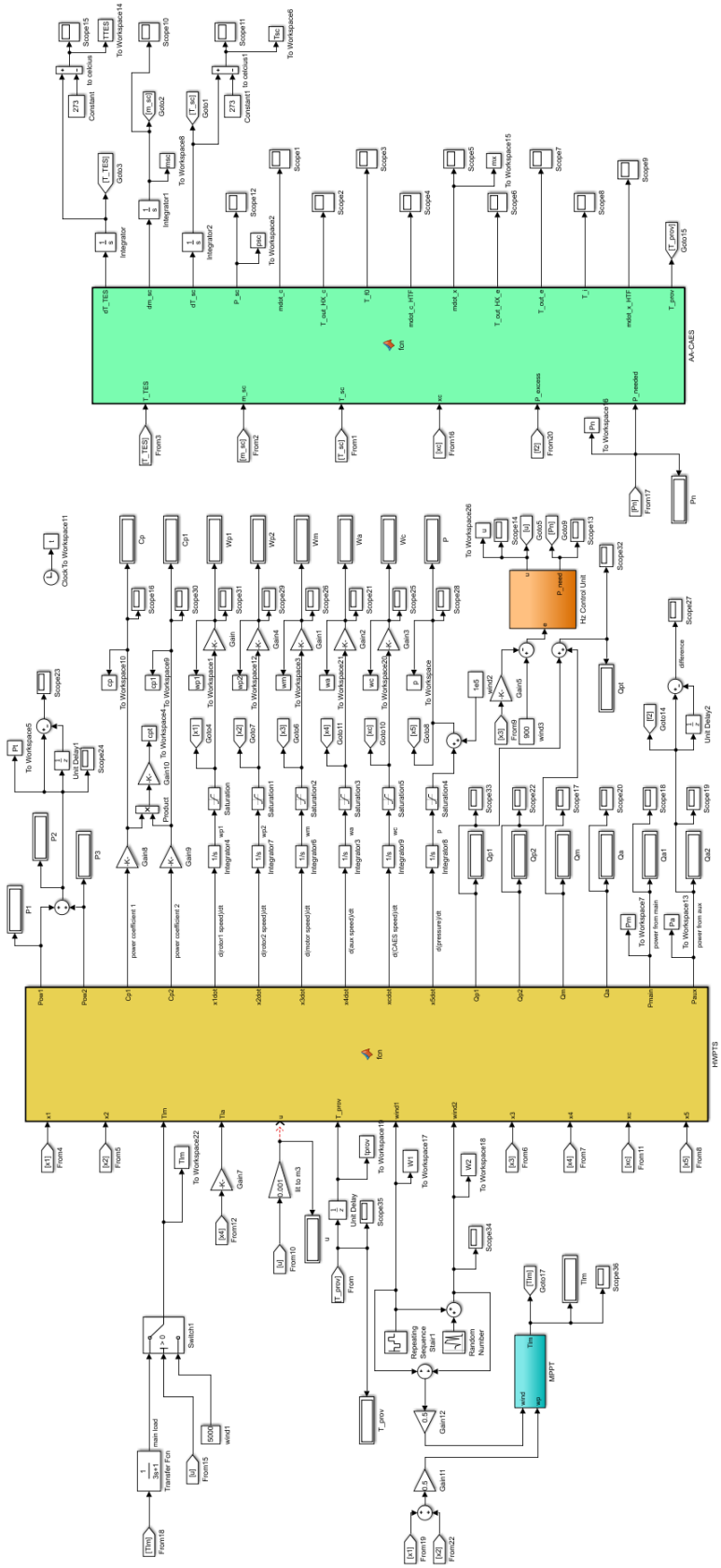

Fig. A.1. Block Diagram of the System

B. SOURCE CODE

```
%--Power Coefficients--
    lambda1 = x1*22/wind1;
    lambda2 = x2*22/wind2;
    li1 = (1/(lambda1 + 0.08*beta1))-(0.035/(1+beta1^3));
    li2 = (1/(lambda2 + 0.08*beta2))-(0.035/(1+beta2^3));
    Cp1 = max(0.5176 * (116*li1 - 0.4*beta1 - 5) * exp(-21*li1) + 0.0068*lambda1,0);
    Cp2 = max(0.5176 * (116*li2 - 0.4*beta2 - 5) * exp(-21*li2) + 0.0068*lambda2,0);
    %--Input Torque--
    Pow1 = 1059*0.617347*(wind1^3)*Cp1;
    Pow2 = 1059*0.617347*(wind2^3)*Cp2;
    Tr1 = Pow1/(x1);
    Tr2 = Pow2/(x2);
    %--flow, control input, and state space--
    Qp1 = 0.02*x1 - x5*7.2e-10;
    Qp2 = 0.02*x2 - x5*7.2e-10;
    Qp = max(Qp1+Qp2,0);
    Qm = 0.001*x3 + x5*1.35e-9;
    Qa = u*x4 + x5*1.35e-9;
    x1dot = (Tr1 - 1012.2254*x1 - 0.000169*x5 - 0.02*x5)/1320000;
    x2dot = (Tr2 - 1012.2254*x2 - 0.000169*x5 - 0.02*x5)/1320000;
    x3dot = (0.001*x5 - 1.7475212*x3 - 0.00000358*x5 + T_prov - Tlm)/80;
    x4dot = (u*x5 - 1.7475212*x4 - 0.00000358*x5 - Tla)/80;
    xcdot = (T_prov - 1.7475212*xc)/500000;
    x5dot = (1100000000/0.24) * (Qp - Qm - Qa);
    %--power--
    Pmain = Tlm*x3;
    Paux = Tla*x4;
    %--CAES--
    T_env = 293;
    eta_c = 0.88;
    eta_e = 0.8;
    cp_air = 1003.45;
    cp_HTF = 1260;
    %--Compression--
    mdot_c = P_excess * eta_c / (cp_air * T_env * 3.7846);
    T_out_c = 4.7846 * T_env;
    T_out_HX_c = T_out_c + 0.7 * (T_TES - T_out_c);
    T_f0 = T_TES + 0.7 * (T_out_c - T_TES);
```

```
    mdot_c_HTF = ((T_out_HX_c - T_out_c)*cp_air*mdot_c)/(cp_HTF * (T_TES - T_f0));
    %--Expansion--
    T_out_HX_e = T_sc + 0.7 * (T_TES - T_sc); %temp after HX1
    if P_needed==0
    mdot_x=0;
    else
    mdot_x = P_needed / (eta_e * cp_air * T_out_HX_e * 0.4163); %required air mass flow
    end
    T_out_e = 0.70606 * T_out_HX_e; %temp after turbine
    T_i = T_TES + 0.7 * (T_sc - T_TES); %temp of HTF going back to TES
    mdot_x_HTF = ((T_out_HX_e - T_env)*cp_air*mdot_x)/(cp_HTF * (T_TES - T_i)); %HTF mass
flow rate
    T_prov = P_needed / (xc);
    %--TES--
    dT_TES = (mdot_c_HTF * cp_HTF * (T_f0 - T_TES) - mdot_x_HTF * cp_HTF * (T_TES - T_i)
)/(2750 * pi * 1 * 1 * 916);
    %--Air Storage--
    dm_sc = mdot_c - mdot_x;
    dT_sc = (1/m_sc) * (1-1/1.4) * (mdot_c*T_out_c - mdot_x*T_sc);
    P_sc = m_sc * 286.9 * T_sc / (56 * 100000); %in bar
```